



# Research of the flow past bluff body

## Diplomová práce

*Studijní program:* N2301 – Mechanical Engineering  
*Studijní obor:* 2302T010 – Machines and Equipment Design  
*Autor práce:* **Mohamed Kabl**  
*Vedoucí práce:* doc. Ing. Tomáš Vít, Ph.D.





TECHNICAL UNIVERSITY OF LIBEREC  
Faculty of Mechanical Engineering ■

# Research of the flow past bluff body

## Diploma thesis

*Study programme:* N2301 – Mechanical Engineering  
*Study branch:* 2302T010 – Machines and Equipment Design  
*Author:* **Mohamed Kabl**  
*Supervisor:* doc. Ing. Tomáš Vít, Ph.D.



## **DIPLOMA THESIS ASSIGNMENT**

(PROJECT, ART WORK, ART PERFORMANCE)

First name and surname: **Mohamed Kabl**  
Study program: **N2301 Mechanical Engineering**  
Identification number: **S14000597**  
Specialization: **Machine and Equipment Design**  
Topic name: **Research of the flow past bluff body**  
Assigning department: **Department of Power Engineering Equipment**

### **R u l e s   f o r   e l a b o r a t i o n :**

The aim of the thesis is to design and perform experiments to research different regimes of isothermal (or non-isothermal) flow past bluff body. Those experiments should be done in towing tank using methods of flow visualization, thermoanemometry and particle image velocimetry.

Structure of the thesis:

1. Literature overview.
2. Overview of experimental methods.
3. Design, construction and manufacturing of the experimental device.
4. Experiments.
5. Comparison of the experimental results with work of other authors.

Scope of graphic works: **20 pages**  
Scope of work report  
(scope of dissertation): **45 pages**  
Form of dissertation elaboration: **printed**  
Language of dissertation elaboration: **English**  
List of specialized literature:

[1] **ZDRAVKOVICH, M. M., 1997.** *Flow Around Circular Cylinders Volume 1: Fundamentals.* Oxford University Press.

[2] **PROVANSAL, M., SCHOUVEILER, L., and LEWEK, T., 2004.** *Eur. J. Fluid. Mech.B/Fluids, vol 23/1.*


[3] **WILIAMSON, C. H. K., 1989.** *Oblique and parallel modes of vortex shedding in the wake of a circular cylinder at low Reynolds numbers.* *J. Fluid Mech.* 206.

[4] **LEWEKE, T., PROVANSAL, M., 1995.** *The flow behind rings: bluff body wakes without end effects.* *J. Fluid Mech.* 288.

Tutor for dissertation: **doc. Ing. Tomáš Vít, Ph.D.**  
Department of Power Engineering Equipment  
Dissertation Counsellor: **Ing. Petra Dančová, Ph.D.**  
Department of Power Engineering Equipment  
Date of dissertation assignment: **18 November 2015**  
Date of dissertation submission: **18 February 2017**

  
prof. Dr. Ing. Petr Lenfeld  
Dean



  
doc. Ing. Václav Dvořák, Ph.D.  
Head of Department

Liberec, dated: 18 November 2015

## Prohlášení

Byl jsem seznámen s tím, že na mou diplomovou práci se plně vztahuje zákon č. 121/2000 Sb., o právu autorském, zejména § 60 – školní dílo.

Beru na vědomí, že Technická univerzita v Liberci (TUL) nezasahuje do mých autorských práv užitím mé diplomové práce pro vnitřní potřebu TUL.

Užiji-li diplomovou práci nebo poskytnu-li licenci k jejímu využití, jsem si vědom povinnosti informovat o této skutečnosti TUL; v tomto případě má TUL právo ode mne požadovat úhradu nákladů, které vynaložila na vytvoření díla, až do jejich skutečné výše.

Diplomovou práci jsem vypracoval samostatně s použitím uvedené literatury a na základě konzultací s vedoucím mé diplomové práce a konzultantem.

Současně čestně prohlašuji, že tištěná verze práce se shoduje s elektronickou verzí, vloženou do IS STAG.

Datum: 27/5/2016

Podpis: 

## **Annotation**

This thesis is dealing with the flow past circular cylinder and the phenomenon accompanying it. It deals with the von Karman vortex in different regimes of flow. It is concentrating also about the approach followed to design and manufacture the experimental device which was used to get the results. An overview about the experimental methods which are pertinent to the flow measurement and visualization was introduced in this thesis. Some methods were used during the measurement procedure and the other methods are going to be used during the future work. A validation and comparison is presented between the current thesis experimental work and the previously done works by another authors.

## **Key Words**

von Kármán vortex shedding, Flow visualization, PIV, Thermo-anemometry, Reynolds number, Strouhal number.

## **Acknowledgment**

I would like to express my sincere gratitude for my supervisor doc. Ing. Tomáš Vít, Ph.D. starting from the first day, his unwavering support, gaudiness and precious instructions throughout this diploma thesis never stopped. I am truly grateful for his aid and support during the whole master degree not only the diploma thesis.

I would also like to say that without the unlimited support from my dissertation counselor Ing. Petra Dančová, Ph.D. it wouldn't be possible to finish this work. She supported me with her experience and time at every step during my work.

I would like to say to my family thank you for believing in me and supporting me in all aspects. You are my real key of success.

## Table of Contents

|   |  |    |
|---|--|----|
| 1 | Chapter One: Introduction .....                              | 14 |
|   | 1.1 Overview .....   | 14 |
|   | 1.2 Outline .....  | 17 |
| 2 | Chapter Two: Literature Review .....                         | 19 |
|   | 2.1 Overview .....   | 19 |
|   | 2.2 Historical Review .....                                  | 19 |
|   | 2.3 Recent Development.....                                  | 22 |
| 3 | Chapter Three: Theoretical overview .....                    | 24 |
|   | 3.1 Conservation Laws .....                                  | 24 |
|   | 3.2 Vortices and the equations of motion.....                | 25 |
|   | 3.3 Vortex shedding and wake hydrodynamics.....              | 26 |
|   | 3.4 Regimes of vortex shedding .....                         | 27 |
|   | 3.5 Drag forces and lifting forces review .....              | 28 |
| 4 | Chapter Four: Experimental Methods .....                     | 29 |
|   | 4.1 Tin Ion Electrolysis .....                               | 29 |
|   | 4.2 Particle Image Velocimetry (PIV).....                    | 31 |
|   | 4.2.1 Analysis .....   | 32 |
|   | 4.3 Thermoanemometry.....                                    | 33 |
|   | 4.3.1 Principle .....  | 34 |
| 5 | Chapter Five: Design and construction of the experiment..... | 38 |
|   | 5.1 Experimental apparatus and techniques .....              | 38 |
|   | 5.2 DC Motor.....  | 41 |
|   | 5.3 Laser Device .....                                       | 42 |
| 6 | Chapter Six: Results and Discussion.....                     | 43 |



|     |   |    |
|-----|---|----|
| 6.1 | Experiment at $Re = 30$ .....   | 43 |
| 6.2 | Experiments at $Re = 50$ .....  | 44 |
| 6.3 | Experiments at $Re = 90$ .....  | 46 |
| 6.4 | Experiments at $Re = 130$ .....   | 47 |
| 7   | Chapter Seven: Comparison of current results with previous authors results..... | 50 |
| 7.1 | Future work.....  | 55 |
| 8   | References .....  | 57 |

## List of Figures

|   |    |
|---|----|
| Figure 1: Relation between drag force and body shape.....   | 16 |
| Figure 2: Proposed vortex system.....   | 20 |
| Figure 3: Schematically representation of the vortex-shedding process .....                                 | 27 |
| Figure 4: Terminology for the cylinder near-wake Kieft 2000.....  | 26 |
| Figure 5: Regimes of fluid flow across circular cylinder .....  | 27 |
| Figure 6: a) Illuminated hydrogen bubbles, b) electrolysis circuit .....                                    | 30 |
| Figure 7a: PIV method setup .....   | 32 |
| Figure 7b: Cross-correlation of a pair of two singly exposed recordings.....                                | 32 |
| Figure 8: Thermo-anemometry probe.....  | 34 |
| Figure 9: Signal processing in thermo-anemometry.....   | 35 |
| Figure 10: Wheatstone bridge circuit.....   | 35 |
| Figure 11: Towing tank.....   | 38 |
| Figure 12: Construction of the end cylinders and the end plates.....  | 39 |
| Figure 13: Experiment design in vertical cylinder mode.....   | 40 |
| Figure 14: the Experiment in Horizontal cylinder mode .....   | 41 |
| Figure 15: a) DC motor components, B) power supply.....   | 42 |
| Figure 16: a) Mounted laser device, b) slotted Adhesive aluminum tab on the laser lamb .....                | 42 |
| Figure 17: Side view of the vortex shedding form the cylinder movement at $Re=30$ .....                     | 43 |
| Figure 18: $Re= 30$ top view of the vertical cylinder span wise vortex shedding.....                        | 44 |
| Figure 19: Stream wise view of the vortex shedding street from the cylinder linear motion at $Re=50$ .....  | 45 |
| Figure 20: Span wise view for the wake of the cylinder at $Re =50$ flow from right to left.....             | 45 |
| Figure 21: Stream wise view of the vortex shedding street from the cylinder linear motion at $Re=90$ .....  | 46 |
| Figure 22: Span wise view for the wake of the cylinder at $Re =90$ flow from right to left.....             | 47 |
| Figure 23: Stream wise view of the vortex shedding street from the cylinder linear motion at $Re=130$ ..... | 48 |
| Figure 24: Span wise view for the wake of the cylinder at $Re =130$ flow from right to lift.....            | 49 |

|  |    |
|--|----|
| Figure 25 Re=30 Comparison of a) numerical and experimental investigations by Masami Sato, b) current experimental results carried out for this thesis.....                    | 50 |
| Figure 26 Relation between separation angle and Reynolds number by several authors (B.N. Rajani, 2009).....  | 51 |
| Figure 27 Variations of Strouhal number vs. Reynolds number by Masami Sato, 2012 .....   | 52 |
| Figure 28: Quasi periodic oblique shedding regime a) current work Re=50, b) Williamson, 1986 Re=64.....  | 53 |
| Figure 29: Periodic oblique shedding mode a) present work Re=90, b) Williamson's work 1986 Re=85.....  | 54 |
| Figure 30: Effect of tilting the end plate on the oblique angle Re=90, Williamson 1986 .....   | 54 |
| Figure 31: Development over one beating cycle of a vortex dislocation near the bottom end of the cylinder span a) present work Re=130, b) Williamson's experiment Re=100 ..... | 55 |

## List of symbols

|                |                        |   |
|----------------|------------------------|---|
| A              | (m <sup>2</sup> )      | Area  |
| d              | (m)                    | Diameter  |
| c              | (1)                    | Constant  |
| S              | (1)                    | Strouhal Number   |
| N              | 1/s                    | Vortex Frequency  |
| U              | (m/s)                  | Velocity  |
| $\vec{V}$      | (m <sup>3</sup> /s)    | Relative variation of volume of a fluid particle in unit time |
| $\vec{f}$      | N/kg                   | Volume force per unit mass                                    |
| T              | (S)                    | Time  |
| $\nu$          | (m <sup>2</sup> /s)    | Kinematic viscosity   |
| $\rho$         | (m <sup>3</sup> /kg)   | Density   |
| $\nabla$       | (1)                    | Laplace operator  |
| Ri             | (1)                    | Richardson number   |
| k              | (m <sup>2</sup> /s)    | Thermal diffusivity   |
| P              | (Pa)                   | Pressure  |
| Re             | (1)                    | Reynolds number   |
| $\Omega$       | (Pa)                   | Potential pressure  |
| $\vec{\omega}$ | (1)                    | Vorticity vector  |
| $\mu$          | (kg/(s·m))             | Dynamic viscosity   |
| I <sub>a</sub> | (1)                    | Image intensity   |
| R              | ( $\Omega$ )           | Resistance  |
| H              | (J)                    | Heat  |
| L              | (m)                    | Length  |
| $\Theta_s$     | (rad)                  | Separation angle  |
| $\lambda$      | (1)                    | Aspect ratio  |
| Nu             | (1)                    | Nusselt number  |
| Pr             | (1)                    | Prandtl number  |
| K              | (W/(m <sup>2</sup> K)) | Heat transfer coefficient                                     |

|       |                         |                                      |
|-------|-------------------------|--------------------------------------|
| $C_p$ | (kJ/kg <sup>0</sup> C)  | Specific heat at constant pressure   |
| $h$   | (W/(m <sup>2</sup> 0C)) | Convective heat transfer coefficient |
| $C_D$ | (1)                     | Drag coefficient                     |
| $C_L$ | (1)                     | Lifting coefficient                  |
| $F_D$ | (N)                     | Drag Force                           |
| $F_L$ | (N)                     | Lifting Force                        |

### List of abbreviations

|      |                                 |
|------|---------------------------------|
| LES  | Large eddy simulation           |
| RANS | Reynolds averaged Navier Stokes |
| PIV  | Particle image velocimetry      |
| CCD  | Charge coupled device           |
| YAG  | Yttrium aluminum garnet         |

# 1 Chapter One: Introduction

Classical fluid dynamics is based on the assumption that the behavior of fluids may be described by considering them as continuous media without taking the motion of their single molecules into account. The physical properties that characterize fluids (and distinguish them from solids) are the lack of a definite shape and the possibility of finite deformation even under the action of infinitesimal forces, provided the latter are properly applied. More precisely, a fluid may be defined as a substance that deforms continuously under the action of tangential stresses. Fluids comprise both liquids and gases, but this distinction is much less fundamental from the dynamical point of view. The main difference between them lies in their elasticity or compressibility. Indeed, gases may be compressed much more easily than liquids, so that any motion that implies significant variations in pressure produces much larger variations in density for gases than for liquids.

The formation and dynamics of the Bénard von Kármán vortex street behind a circular cylinder has been the subject of several hundreds of publications. This very large number is linked to the importance of this type of flow for applications in different engineering fields and to the apparent simplicity of this configuration. By mere observation Leonardo da Vinci produced accurate drawings of the turbulent structures in a water flow. Not a trivial task considering the many scales and the temporal variation present in a turbulent flow. Today, almost five hundred years after Leonardo da Vinci made his drawings, analysis of turbulent flows has become essential to realize significant improvements to the propulsion systems and external configuration of flow disturbances. Improvements which are essential to achieve reductions of greenhouse gasses, fuel consumption and aircraft noise. We can find the great importance of the bluff body fluid dynamics study present in civil engineering, automotive engineering, naval hydrodynamics, air conditioning and ventilation etc.

## 1.1 Overview

Starting from Prandtl and von Kármán's early works on the field of fluid dynamics there has been an enormous amount of research dedicated to the study of flows around bluff bodies. The mechanisms of flow separation, vortex formation, the behavior of the wake and fluid structure

interaction constitute some of the most important as well as classical problems in fluid mechanics. Considering the overwhelming number of publications and research hours dedicated to the understanding of the aforementioned problems. Unlike what someone think that the redoing the experiments or the tries to understand the flow in this case is a matter of time wasting or useless work in reality the great practical importance of such flows generates better understanding of the fundamental principles that govern these types of flows. In addition, the continuous evolution of experimental, numerical and analytical methods provide us today with new tools to gain a more complete and thorough understanding of such flows.

Anybody moving through viscous medium will face the effect of the drag forces which is usually divided into two components, i.e. frictional drag and pressure drag. Frictional drag also known as *skin friction drag* comes from friction between the fluid and the surfaces over which it is flowing. This friction is associated with the development of boundary layers. The fluid molecules in direct contact with the body surface are most affected. As the molecules flow past the surface and past each other the viscous resistance to that flow becomes a force which retards forward motion. Turbulent flow creates more friction drag than laminar flow due to its greater interaction with the surface of the body. Rough surfaces accelerate the transition of boundary layer airflow from laminar to turbulent. Pressure drag comes from the eddying motions that are starting to happen at the wake of the body. The air pressure against the leading side of an object is higher than the pressure in the randomly churning eddies of the wake on the other side of it. Streamlining reduces this pressure difference.

Frictional drag is important for attached flows which do not have separation and it is related to the surface area exposed to the flow. Pressure drag is important for separated flows, and it is related to the cross-sectional area of the body. When the drag is happening due to viscosity of the fluid, we say the body is streamlined. When it is dominated by the pressure of the drag, we say the body is bluff. Whether the flow is viscous-drag dominated or pressure drag dominated it depends mainly on the shape of the body, see fig. (1).

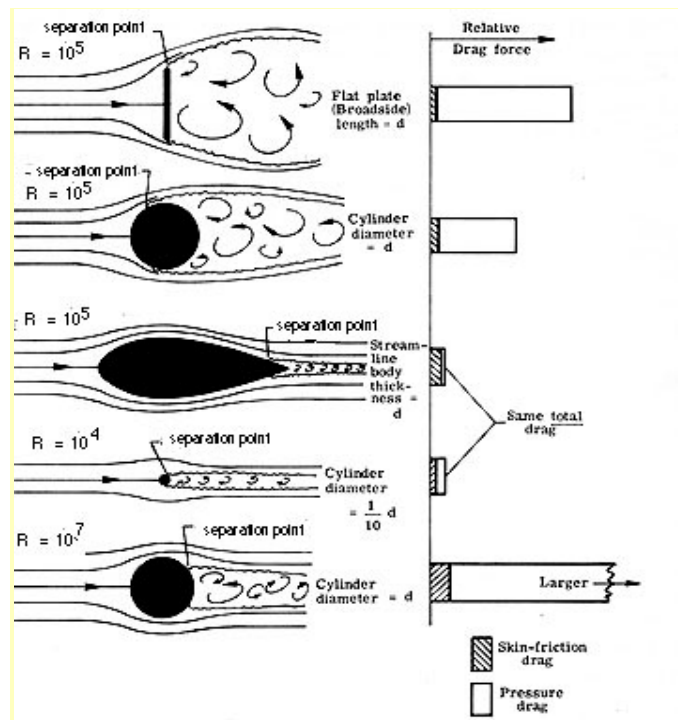


Figure 1: Relation between drag force and body shape  
[http://www.pilotfriend.com/training/flight\\_training/aero/aero\\_res.htm](http://www.pilotfriend.com/training/flight_training/aero/aero_res.htm)

For streamlined bodies, frictional drag is the dominant source of fluid resistance however, for bluff body the dominant source of drag is pressure drag. For a given frontal area and velocity a streamlined body will always have a lower resistance than a bluff body. Cylinders and spheres are considered bluff bodies because at large Reynolds numbers the drag is dominated by the pressure losses in the wake. The vortex shedding frequency  $n$  (Hz) is normally presented in non-dimensional form as Strouhal number,  $St$ , where  $St = \frac{n \cdot D}{U}$ ,  $D$  (m) is the diameter of the cylinder of sphere and,  $U$  (m/s) is the fluid velocity. The value of the Strouhal number varies from one bluff body to another and, as in the case of a circular cylinder, it may change with changing  $Re$ . A small improvement in drag could have dramatic cost savings for applications like trucks or boats where fuel consumption per kilometers would decrease as drag is reduced. For these objects, a passive drag reduction technique is the simplest and most cost effective way of reducing drag at a particular Reynolds number.



## 1.2 Outline

This thesis is mainly intending to cover the flow visualization and the experimental methods for the flow around circular cylinder (bluff body) which can serve in getting the best result with lowest losses according to the available material. And experimental mechanism was developed in order to perform the experiment in the technical measurements laboratory. The first chapter gives an overview about the topic of fluid flow around bluff bodies and the basic terms which is used in the field. Briefly, the overview scoop on the basics of the fluid mechanics laws pertinent to the fluid flow around bluff bodies and the characteristics of such flows like this.

Chapter two presents a literature review about the topic of fluid flow around bluff body and the recent works and publication including the results and techniques used to explain the status of the flow. It shows a series of works done by scientists in order to solve the secrets of this topic since it was a little bit vague topic till a very close time in the science history. The importance of this topic arises since the industrial revolution in the 19th century. Also I tried to concentrate about the last five years from both the simulation and experimental works to show how developed have this field reached and what are the areas of development and research which needs a special concentration. The amount of publications and researches doe in this area is considerably big due to its importance and lake of understanding for it phenomenon in the same time.

Theoretical background about the vortex hydrodynamics and the mean phenomena accompanying its occurrence is explained in details in chapter three. The equations of motion of the flow in addition to, the hydrodynamics principle of the vortices formation and shedding are explained in this chapter. Several regimes of vortex shedding are reviewed.

After that, in chapter four I focused on the design, construction and manufacturing of the experimental device consideration I followed to perform the experiment. A detailed explanation of the design dimensions and techniques used to get the result and the reason for choosing these components. I used some previous experimental consideration and theoretical recommendations about the optimum dimensions and design suitable to make the experiment and to avoid the problems which may cause bad results. Some material was already in the laboratory so the

experimental device was designed in somehow which allow me exploit this facilities as much as I can.

In chapter five, an overview about the experimental methods used during the experimental work and also the methods which could be used in the future works. An explanation for the components and the principle of these experimental methods used in addition to theoretical background for the design of these experimental methods used to perform the experiment and get the results. The experimental methods were from the fields of flow visualization, velocity measurement and temperature measurements. Other experimental methods might be added for the future works which is not mention here at the present work.

A detailed explanation of the results achieved during the experiment was mentioned in chapter six. A different orientation of the experiment setup used to get different results in several planes and position in order to screen several phenomena accompanying the flow around the bluff body. A theoretical explanation also is provided for the flow configurations observed during the measurements and the possible reasons which led to it according to the theoretical principles of the von Kármán vortex shedding and the flow around bluff bodies.

Finally, a comparison between experiments which was carried out in this thesis and a works published previously by another authors in similar topics is made in chapter seven. Some validation for the results got by the experimental work and explanation for what is reason for the conflicts between the experiment results got and the other author's experimental and numerical results and hypothesis. In this chapter, the outline of the future work is also described.

## 2 Chapter Two: Literature Review

### 2.1 Overview

Bluff bodies studies are essential for the understanding of fluid dynamics phenomenon and configurations around bluff bodies and the effect of these flows on the body or vice versa. It has wide range of applications in several industries and fields. Bluff body objects are common in many applications including: tractor trailers, aft sections of large vehicles, helicopter fuselages, large transport aircraft, and reusable spacecraft capsules. The problems of bluff body drag forces has been discussed in the literature over the past fifty years by many scientists in order to use the advantages of it in some application and exclude it in some other.

### 2.2 Historical Review

The bluff body topic wasn't until 1878, when Strouhal published his pioneer paper on singing wires caused by vortex shedding, that this type of flow became a subject of quantitative research. Since this time a lot of researchers started to study this simple shaped and complex flow phenomenon topic, [1]. Theodore von Kármán was the first one to stimulate widespread interest and publish the first theoretical study of vortex streets in 1911, [2]. (Schatzman, 1981), who studied the analysis of a model for the *von Kármán vortex street* found that the linear stability of the point vortex has been generalized to vortices of finite size and can stabilize the array, [3].

Ahmed et al. observed that for a base slant angle less than  $30^\circ$  a separating shear layer turns up from the sides of the rear slanted edge of the bluff body designed and rolls into two longitudinal vortices. Also the flow separates from the roof and then reattaches on the slant near the vertical base forming an arch-shaped separation vortices over the surface (Vino et al., 2004), [4]. After leaving the rear of the designed body the flow again separates from the top and bottom edges of the vertical base, forming two separation bubbles, one above the other and in opposing directions.

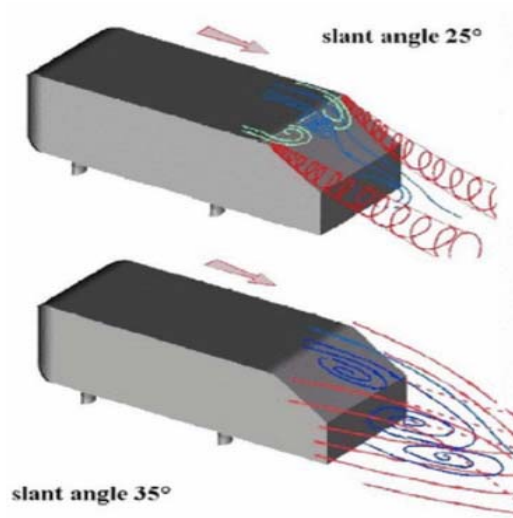


Figure 2: Proposed vortex system, Ahmed et al. 1984

In (1987) Provansal et al, [5] found that the periodic vortex street near the wake is the saturated end product of temporal global wake instability, and not a spatial response to continuously supplied upstream disturbances. They also showed that the wake dynamics could be described by a single Stuart-Landau (SL) equation by measuring all coefficients of the SL-equation for a range of Reynolds numbers near the onset of Kármán shedding. They recalled briefly the place of the Landau model in hydrodynamics. The approach starts from the attempt to perform the stability analysis of a steady flow. A non-stationary perturbation  $u(x, y, z, t)$  of the steady solution  $u(x, y, z)$  of the Navier-Stokes equations is expanded as a sum:

$$U_1(x, y, z, t) = \sum \{A_i(t) g_i(x, y, z) + A_i(t) g_i(x, y, z)\}, i=1 \quad (1.2)$$

where,  $g_i(x, y, z)$  satisfies the boundary conditions.

Bearman & Trueman (1972), [6] and Mizota & Okajima (1981), [7] used 2-D rectangular cylinders with various side ratios to investigate the drag forces caused due to the formation position of the Kármán vortices and they found that the close formation of the rectangular rear faces make the drag force large. They also introduced an explanation of the Nakaguchi peak (Nakaguchi et al. 1968) of the drag force of a 2-D rectangular cylinder with the specific side ratio of 0.64.

Williamson (1986) [8], studied various complicated shapes and regimes of Kármán vortex shedding like as oblique shedding modes and also he studied the 3-D characteristics around 2-D circular cylinders at a reasonably low Reynolds numbers. Furthermore, Shimada & Meng found that Kármán vortex shedding is quite weak or not existing at the critical side ratios of 2.8 and 6.0 for 2-D rectangular cylinders by means of advanced CFD analysis. The Strouhal number suddenly changes with varying side ratio [9]. Matsumoto et al. (1988) reported that the Strouhal number associated with Kármán vortex shedding is dependent on the angle of attack, which modifies the flow pattern around the body, for 2-D rectangular cylinders with a side ratio of 2.0,[10].

P.J. Strykowski in [11] used cylinder in the rear of the flow past circular cylinder over a limited range of Reynolds numbers in order to control the vortex shedding which will result in a superposition of the vortex. It was doubted that the cylinder in the wake may affect the flow by altering the local stability through diffusing the concentrated vortices in the shear layers behind the cylinder.

Choi, Haecheon et al. did his experiment to reduce the drag forces by means of controlling the vortex shedding using active or passive flow control devices. For the low Reynolds numbers it was observed that the Kármán vortex shedding can be suppressed because the 3-D redistributed shear layers become less susceptible to rolling up into a Kármán vortex street, [12]. Park et al. [13] stated that the use of tabs was highly effective at drag reduction on 2D bodies.

Martyn Paley et al. [14] investigated the flow regime with strong transient characteristics including vortex shedding and transport for the purpose of developing new methodologies which are appropriate to the analysis of carotid stenosis. The model which was chosen in the study for both ease of phantom construction and of theoretical modeling using finite element computational fluid dynamics (CFD). He compared the theoretical calculations with two methods of flow visualization, the first one was laser sheet imaging and the second was real-time echo planar magnitude MR imaging. Flow was investigated over a range of Reynolds number from 40 through 400 through which vortex shedding is predicted.

Rindt et al in [15] studied the wake behind a horizontally mounted heated cylinder with circular cross-section experimentally. It was visualized using tin precipitation method. He used

towing tank to perform his experiments. In the experiments mean Reynolds number  $Re_D$  and mean Richardson number  $Ri_D$  both based on main stream properties, were set to  $Re_D = 117$  and  $Ri_D$  value was varied between 0 and 1.5. The wake becomes 3D from  $Ri_D = 0.3$ .

In 2006 T.vit et al. studied the wake past a heated circular cylinder in the laminar vortex shedding regime. Water was used as the working fluid to perform the experimental study of the wake flow behind a heated cylinder in the forced convection regime. Flow visualization experiments were performed in addition to hot-wire anemometry was used for  $St-Re$  data acquisition. Data analysis confirmed the so-called thermal effect in water. It was discovered that cylinder heating increases the vortex shedding frequency and destabilizes the wake flow. The  $St-Re$  data were successfully transformed to the  $St-Re_{eff}$  curve and the effective temperature concept was used, [16].

Detailed computations have been carried out for variation of wake flow pattern by Rajani.B.N. et al. [17]. The mean drag coefficient, variation of the position of the separation points with variety of Reynolds number in addition to the corresponding frequency and amplitude of the fluctuating forces arising out of the phenomenon of vortex shedding. They have used pressure based finite volume algorithm (RANS3D) for time accurate prediction of the flow through numerical solution of Navier Stokes equations.

### **2.3 Recent Development**

Venugopal et al. studied various bluff body shapes experimentally and numerically in order to identify the most appropriate shape which can be used for vortex flow meter application.  $k-\epsilon$  RNG model predicted the Strouhal number closer to the experimental results than other models. It was found also that the axisymmetric tapping is better than differential pressure tapping. The trapezoidal bluff body gave the best results among all the bluff bodies investigated in terms of signal amplitude and constancy of Strouhal number. Using gate valve and bends, the vortex flow meter performance is also measured under disturbed flow conditions, [18].

Fluid flow around a circular cylinder placed in a uniform flow was investigated in addition to the occurrence of various phenomena associated with von Kármán vortices and the oscillation of a circular cylinder excited by these vortices over the object using Abaqus/CFD by Masami Sato et al., [19].

Zaaraoui et al. invented device for measuring the volume by counting vortices. It consisted of a quadrangular pipe section in which are placed a two-dimensional bluff body and a strain gauge force sensor. The principle is based on the generation of a separated wake behind the bluff body. The volume measurement is done by counting vortices using a flat plate placed in the wake and attached to the beam sensor. In the case of volume measurement, the constant of the device which is called digital volume ( $V_p$ ) varies with the confinement of the flow vein and with the Reynolds number, [20].

L. Cheng et al. obtained the fluctuating characteristics of building wakes through measurement of unsteady velocity fields with time resolved particle image velocimetry (PIV), [21]. Hui Liang et al. [22], numerically investigated the span wise characteristics of flow passing a yawed finite circular cylinder at the yawed angle of  $30^\circ$ , aspect ratio of 9 and Reynolds number of 3900 using Large Eddy Simulation. The cylinder was assumed to be divided into nine equally spaced sections along the cylinder span. The drag and lift force coefficients of each section was monitored. The anticlockwise torque was found to be imposed on the cylinder. By comparing the drag coefficients of these nine cylinder sections.

Siddhartha investigated experimentally the flow field of air in a rectangular diffuser with different inlet velocity. He deduced the displacement thickness and momentum thickness by numerical integration. He found that the boundary layer thickness is lower for higher inlet velocity moreover; He found that Displacement thickness is fluctuating at upstream and top of bluff body while at downstream side it decreases with increase of inlet velocity. He found also that momentum thickness is inversely proportional with the increase inlet velocity. The variation of momentum thickness is higher for high inlet velocity, [23].

Caetano and van der Laan studied experimentally, turbulent flow fields stabilized on the Bluff Body burner. Measurements were performed using non-intrusive optical technique in order to yield the velocity field, employing PIV. Vector velocity field is performed, employing Particle Image Velocimetry technique. Also an uncertainty analysis is performed considering parameters involved in this technique, [24].

### 3 Chapter Three: Theoretical overview

The equations of fluid dynamics may be obtained by expressing in mathematical terms the three fundamental balances equations.

- The conservation of mass (or continuity equation)
- The momentum balance (or fundamental Newton law)
- The balance of energy (or first principle of thermodynamics)

#### 3.1 Conservation Laws

With the assumption of incompressibility it may be shown that the conservation of mass for a fluid particle is expressed by the following linear differential equation, [25].

$$\text{div } \vec{V} = \frac{\partial u}{\partial x} + \frac{\partial v}{\partial y} + \frac{\partial w}{\partial z} \quad (1.3)$$

where  $\text{div } \vec{V}$  is the relative variation of volume of a fluid particle in unit time. The equation for the balance of momentum of an incompressible fluid in vector notation is the following:

$$\frac{\partial \vec{V}}{\partial t} + \vec{V} \cdot \nabla \vec{V} = \vec{f} - \frac{1}{\rho} \nabla P + \nu \nabla^2 \vec{V} \quad (2.3)$$

where  $\vec{f}$  is the volume force per unit mass acting on the particle and  $\nu$  is the so called kinematic viscosity of the fluid, and  $\nabla^2$  is the Laplace's operator. The two terms in the left-hand side may be shown to express the variation in time of the velocity of a fluid particle. The first one is the so-called unsteady term while the second is the convective term giving the variation of velocity of a particle due to its transport by the velocity field through a gradient of velocity. In the right hand side all terms are forces per unit mass acting on the particle: the first corresponds to volume forces and the remaining ones to the resultant of the surface forces, divided in two terms corresponding one to pressure and the other to the viscous stresses. Considering the flow in 2-D Cartesian coordinates we can consider the momentum equations in the form

For momentum in x-axes

$$\frac{\partial V_x}{\partial t} + \frac{\partial(V_x V_x)}{\partial x} + \frac{\partial(V_y V_x)}{\partial y} = \frac{\partial P}{\partial x} + \frac{1}{Re} \left( \frac{\partial^2 V_x}{\partial x^2} + \frac{\partial^2 V_x}{\partial y^2} \right) \quad (3a.3)$$



For momentum in y-axes

$$\frac{\partial V_y}{\partial t} + \frac{\partial(V_x V_y)}{\partial x} + \frac{\partial(V_y V_y)}{\partial y} = \frac{\partial P}{\partial y} + \frac{1}{Re} \left( \frac{\partial^2 V_y}{\partial x^2} \frac{\partial^2 V_y}{\partial y^2} \right) \quad (3b.3)$$

We can express the energy equation the form of

$$\frac{\partial T}{\partial t} + \frac{\partial(V_x T)}{\partial x} + \frac{\partial(V_y T)}{\partial y} = K \left( \frac{\partial^2 T}{\partial x^2} \frac{\partial^2 T}{\partial y^2} \right) \quad (4.3)$$

### 3.2 Vortices and the equations of motion

In order to get better understanding of the theoretical approach it is appropriate to analyze more the mathematical and physical aspects of the motion. So we can stat the vorticity vector

$$\vec{\omega} = \text{curl } \vec{V} = \nabla \cdot \vec{V} \quad (5.3)$$

From the definition, it may be seen that in quite general conditions the velocity field may directly be derived from the knowledge of the vorticity field. It is also easy to show that the value of the vorticity in a point is equal to twice the angular velocity of the fluid particle occupying that point. More importantly, it is not necessary that this quantity be present in the whole field, and its distribution and dynamical behavior determines the values of the forces acting on bodies immersed in the fluid. Finally, by introducing vorticity, the equations of motion may be given a form that may be very useful to understand the role of the various terms and to devise solution procedures. The following expression can apply

$$\vec{V} \cdot \nabla \vec{V} = \vec{\omega} \cdot \vec{V} + \nabla \left( \frac{V^2}{2} \right) \quad (6.3)$$

Assuming that the volume forces is conservative

$$\vec{f} = - \nabla \Omega \quad (7.3)$$

So we can write the momentum equation in the following form

$$\frac{\partial \vec{V}}{\partial t} + \vec{\omega} \cdot \vec{V} = -\nabla \left( \frac{V^2}{2} + \frac{P}{\rho} + \Omega \right) - \nu \text{curl } \vec{\omega} \quad (8.3)$$

It may be seen that if the motion is irrotational then the last term in the equation, connected with viscosity, vanishes. If the motion, besides being irrotational, is also steady, then the first term vanishes also and Bernoulli equation holds in the field

$$\frac{V^2}{2} + \frac{P}{\rho} + \Omega = c \quad (9.3)$$

### 3.3 Vortex shedding and wake hydrodynamics

The process in which boundary-layer produced vorticity organizes into a coherent vortex structure takes place within the so-called formation region. This region is the area downstream of the cylinder and its downstream end is denoted by the formation length  $L_f$  which is based on the position for which the vorticity contours form a closed contour around the structure. In the formation region other characteristic areas or points can be defined. In the very near wake the flow recirculates. Therefore a recirculation region with length  $L_r$  can be defined for which the average motion within the area enclosed by  $L_r$  shows a double recirculation pattern. A shed vortex is then defined as the area with a local vorticity extreme  $\omega_{ext}$  bounded by the closed vorticity contour of the value  $0.1 \omega_{ext}$ , [26]. Furthermore, on the cylinder surface one can find two stagnation points  $St_1, St_2$  and two boundary layer separation points  $Sp_1, Sp_2$ , see figure 3

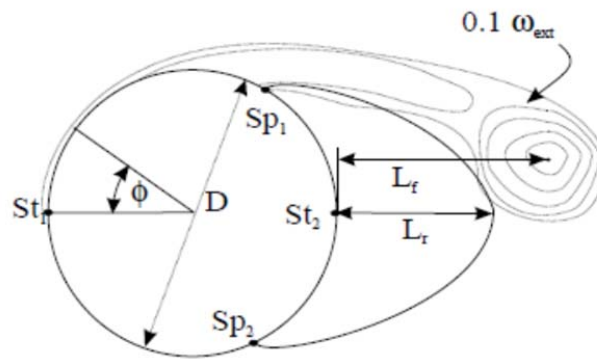


Figure 3: Terminology for the cylinder near-wake Kieft 2000

Within this near wake the vortex formation and shedding process takes place. According to Green and Gerrard this process can be thought to be divided into three distinguishable stages. The first stage concerns the accumulation of the boundary-layer produced vorticity, resulting in the emergence of a coherent blob of vorticity at the tip of the strand. In the second stage, the separation of this blob from its own source, the boundary layer, takes place. At a certain moment, upstream of the strand tip, a constriction process is initiated. The final stage of the formation process is the actual shedding. As soon as the constriction has been accomplished the vortex structure is accelerated in the downstream direction and leaves the formation region, see fig. (3).

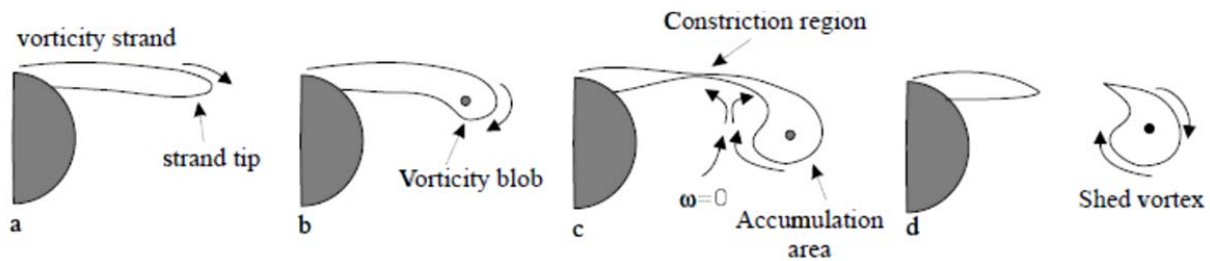


Figure 4: Schematically representation of the vortex-shedding process as suggested by Green and Gerrard (1993)

### 3.4 Regimes of vortex shedding

It was observed the presence of several regimes of von Kármán vortex shedding with the variation of Reynolds number. The flow regimes determine the shape and hydrodynamics characteristics of the flow past the cylinder, [27]. The flow regimes can be divided to four main categories as a function of Reynolds number. In figure five we can see that the flow which has  $Re < 5$  is called regime of unseparated flow (creeping flow). Eddies remain steady and symmetrical but grow in size up to a Reynolds number of about 40. At Reynolds number above 40 oscillations in the wake induces asymmetry and finally the wake starts shedding vortices into the stream. This situation is termed as onset of periodicity the wake keeps on undulating up to a Reynolds number of 90. The periodicity is governed at this range by wake instability. At Reynolds number above 90 the eddies are shedding alternately from a top and bottom of the cylinder and the regular pattern of alternately shed clockwise and counterclockwise vortices form von Kármán vortex street. The periodicity in this range is governed by the vortex shedding street. At  $150 > Re > 300$  the flow starts to turn to turbulence in the vortex. At  $Re = 300$  the vortex street becomes fully turbulent and vortex periodicity vanishes completely in distance  $48D$ , see fig. (4).

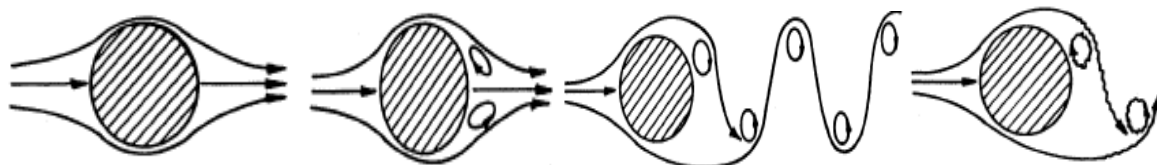


Figure 5: Regimes of fluid flow across circular cylinder, John H.Lienhard, 1966.

### 3.5 Drag forces and lifting forces review

Extensive reviews of this subject are given by Clift (1978), and Yoshida et al (1979). Conventionally, aerodynamic force can be classified into two components: drag, in the direction of the mean flow; and lift, perpendicular to it. For uniform flow over a particle, the drag force is expressed by

$$F_D = \frac{C_D \rho U^2 A}{2} \quad (10.3)$$

And for the lifting force we can express it in the following form

$$F_L = \frac{C_L \rho U^2 A}{2} \quad (11.3)$$

These equations can also be used in a stationary fluid for a steady translating body, where  $U$  is the body velocity instead of the fluid velocity, since  $U$  is still the relative velocity of the fluid with respect to the body.

The drag force arises due to viscous rubbing of the fluid. The fluid may be thought of as comprised of several “layers” which move relative to one another. The layer at the surface of the body “sticks” to the surface due to the no-slip condition. The next layer of fluid away from the surface rubs against the layer below, and this rubbing requires a certain amount of force because of viscosity.

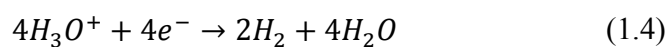
## 4 Chapter Four: Experimental Methods

In order to describe the flow of past circular cylinder bluff body certain types of flow investigation methods should be used to help in evaluation the variable accompanying the flow. The types of the flow investigation techniques are varied between flow visualization methods, velocity and temperature investigation methods. Certain types also are used to determine the frequency of the vortex past bluff bodies. In this chapter the methods of tin ion perception method is explained. Particle image velocity meter (PIV) as a method to find the velocity of the particles of the flow. Another temperature investigation method explained which is so called thermo anemometry.

### 4.1 Tin Ion Electrolysis

In order to get qualitative information about the flow field fluid flow visualization experiments can be performed. Flow visualization includes the study of techniques to display dynamic behavior in liquids and gases and making these patterns visible. In experimental fluid dynamics, flows can broadly be visualized using three main methods: surface flow visualization techniques, particle/molecule tracer methods and optical methods. Surface flow visualization reveals the flow streamlines in the limit as a solid surface is approached. Particles similar to smoke can be added to the flow to trace fluid motion. Illuminating the particles in a fluid with a sheet of laser light has been used widely in order to visualize a complicated flow field. flow visualization has become more exact and precise with careful control of the particulate size and distribution. Advances in photography have also helped in extending our understanding of various flow fields. In this way insight into the various flow phenomena can be obtained, useful for example for planning more detailed quantitative experiments. Within this research project Tin ion Electrolysis method were used as a method of flow visualization, [28].

In Tin ion Electrolysis experiments, small gas bubbles are generated to visualize the flow. The bubbles are created by the process of electrolysis perception. When a potential difference is applied, hydrogen bubbles are formed at the cathode (negative) side according to the following chemical reaction



At the anode (positive) side oxygen bubbles are formed according to

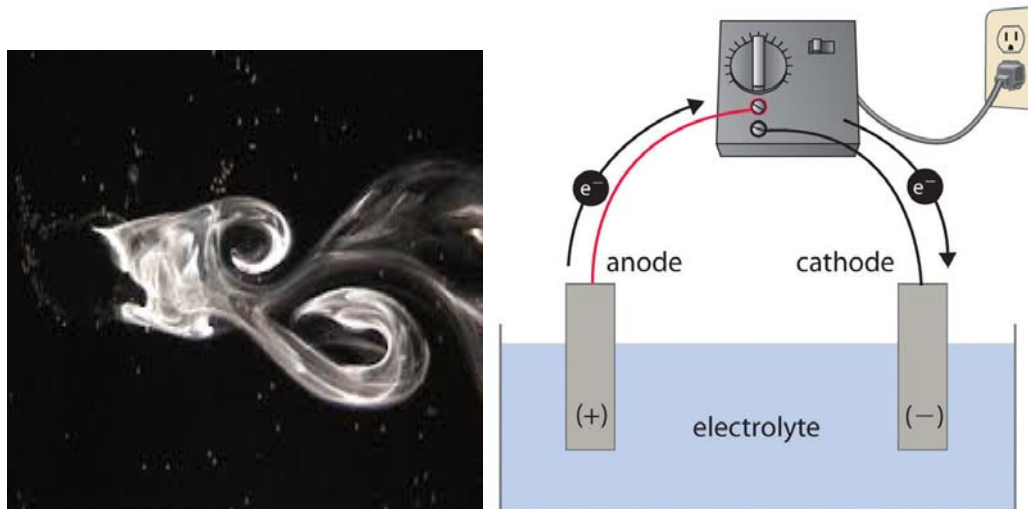
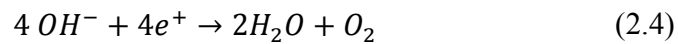


Figure 6: a) Illuminated hydrogen bubbles, b) Electrolysis Circuit by Yukie Tanino

The anode is a tin tube which is connected to the power supply by a wire. Meanwhile the cylinder performs the same task of the bluff body. The cathode can be any inert conductor. Copper works well as a cathode and can be placed anywhere in the fluid where it will not obstruct the flow. Increasing the cathode surface area increases tin production and produces better photographic contrast. A copper mesh can be used for this purpose. The rate of oxide production also increases as the distance between the electrodes is decreased. The circuit is connected to a DC power supply that can be operated simply in short pulses using a simple switch. When the potential difference is applied across the electrodes, an electric current flow and induces tin dissolution from the wire-see fig. (6). The dissolution of tin in the water makes a precipitate of tin oxide that appears as a highly reflective white smoke. We can enhance the contrast by illuminating the oxide cloud by a light sheet. From the chemical point of view the compound is most likely a hydrated tin oxide. Voltages in the range of 10V with currents around 10 mA are typically used. Higher voltages will increase the rate of tracer production, but if the voltage is too high hydrogen bubbles will begin to form. Tap water can be used as the working fluid. While some papers suggest the addition of salt as a means of increasing the fluid's electrolytic conductivity, such additions may result in the production of tin chloride, which is

toxic. Other metals can be used to perform this experimental method like Solder which is commonly suggested, however most solder contain lead, which is toxic. Finally, note that because tin is a heavy metal it must be filtered from the working fluid before releasing it to a drain.

## **4.2 Particle Image Velocimetry (PIV)**

Particle Image Velocimetry is an experimental method that provides two dimensional whole field measurements of the velocity and subsequently the one component vortices distribution in the area under investigation, [26]. In fact, qualitative particle flow visualizations were the first try to visualize and calculate the flow conditions. The first one to state the basics of PIV methods was Meynard. Recently, there is so many developments have been added on the technique as well as applications of the method for a wide range of flows starting from low speed liquid to high speeds and also the simple two phase flows to supersonic gas flows, see fig. (7a).

One of the most common techniques to make the PIV method is to integrate a laser light sheet generated by pulsing lasers that illuminates some interrogation area and a high resolution cross correlation CCD camera. We can receive from this typical configuration up to 15 instants of the flow field per second and over 900 independent vectors. There many advantages for using these methods can be summarized in the following. The use of the YAG lasers provides high energy/pulse ( $>100\text{mJoules/pulse}$ ) light source with good coherence and intensity profile in addition to the fact that the CCD camera has superior signal to noise ratio than the standard photographic film. This can help in excluding the intermediate digitization step, in addition to taking advantage of a fully computer based data acquisition system. Recently developed digital image processing techniques are used to accelerate the evaluation and validation of the flow field. In the digital implementation of PIV the ability to investigate and study, high speed flow fields have been enhanced using the so-called (cross correlation) CCD cameras. It works by acquiring two fields per frame separated only by a few nanoseconds ( $<100\text{ns}$ ). Thus, we can say that double frame single exposure cross-correlation of two consecutive frames became the most popular approach to carry out PIV measurements, see fig. (7b).

Regarding the disadvantage of this approach is the bad ability to examine any high frequency phenomena that occur in turbulent flows because of the inability to provide sufficient time resolution.

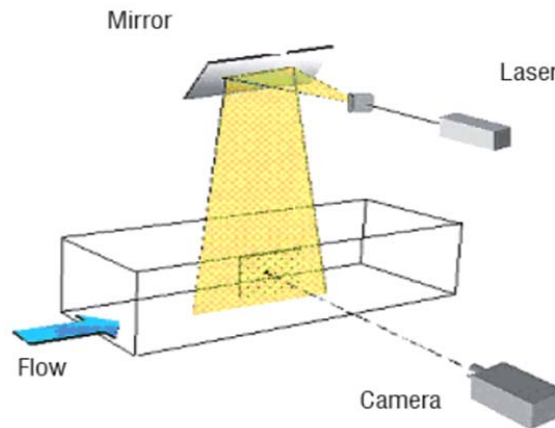


Figure 7a: PIV method setup C. Brossard, J.-C. Monnier 2009

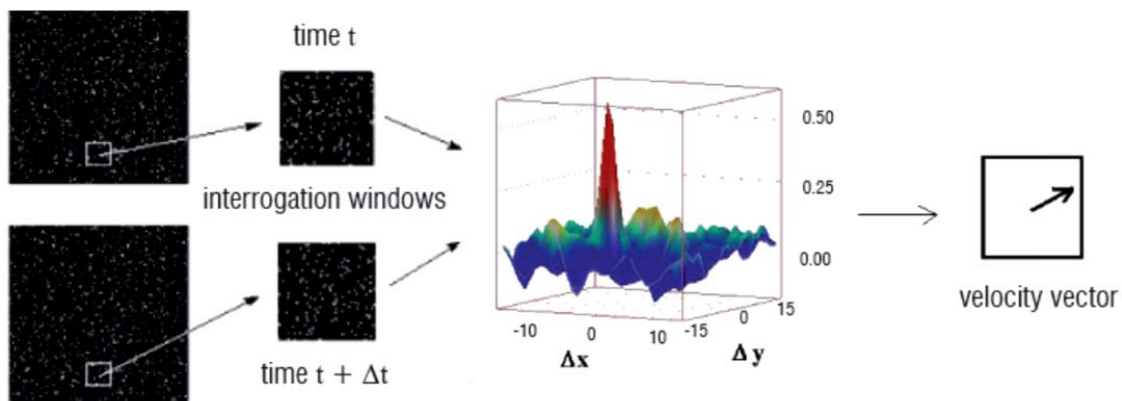


Figure 7b: Cross-correlation of a pair of two singly exposed recordings C. Brossard, J.-C. Monnier 2009

#### 4.2.1 Analysis

The frames are split into a large number of interrogation areas, or windows. It is then possible to calculate and investigate the displacement vector for each window captured with help of signal processing and autocorrelation or cross-correlation techniques, [29]. This is converted to a velocity using the time between laser shots and the physical size of each pixel on the camera. The size of the interrogation window should be chosen to have at least 6 particles per window on average. The image intensity field of the first exposure may be expressed by:



$$I_a = \frac{1}{B_x B_y} \sum_{k=1}^{B_x} \sum_{l=1}^{B_y} (I_a(k, l)) \quad (3.4)$$

And for the second exposure

$$I_b = \frac{1}{B_x B_y} \sum_{k=1}^{B_x} \sum_{l=1}^{B_y} (I_b(k + i, l + j)) \quad (4.4)$$

The cross-correlation of the two interrogation windows is defined as:

$$R(\mathbf{s}) = \langle I(x) I(x + \mathbf{s}) \rangle \quad (5.4)$$

Where  $s$  is the separation vector in the correlation plane, and  $\langle \rangle$  is the spatial averaging operator over the interrogation window, [30].

$R$  can be decomposed into three parts:

$$R(\mathbf{s}) = R_c(\mathbf{s}) + R_f(\mathbf{s}) + R_D(\mathbf{s}) \quad (6.4)$$

Where  $R_c$  is the correlation of the mean image intensities, and  $R_f$  is the fluctuating noise component. The displacement-correlation peak  $R_D$  represents the component of the cross-correlation function that corresponds to the correlation of images of particles from the first exposure with images of identical particles present in the second exposure. Statistical correlations used to find average particle displacement.

$$R(i, j) = \frac{\sum_{k=1}^{B_x} \sum_{l=1}^{B_y} (I_a(k, l) - I_a) (I_b(k+i, l+j) - I_b)}{\sum_{k=1}^{B_x} \sum_{l=1}^{B_y} (I_a(k, l) - I_a) \sum_{k=1}^{B_x} \sum_{l=1}^{B_y} (I_b(k+i, l+j) - I_b)} \quad (7.4)$$

### 4.3 Thermoanemometry

Thermoanemometry is a technique for measuring the velocity and temperature of fluids and can be used in many different fields. It is mainly used due to its advantages specially its good signal sensitivity to the small change in velocities. And also the high frequency response and the low disturbance caused to the flow. It has also wide velocity range and good spatial resolution. In addition to all of these advantages it is so easy to use and relatively cheap method of measurement.

### 4.3.1 Principle

A thermo-anemometer consists of a holder with a wire stretched on it. The wire is usually made of tungsten, platinum or platinum-iridium, [32]. A small, glass coated thermistor bead is often used on constant temperature circuit versions. A thermo-anemometer works as follows: an electric current is sent through the wire, causing the wire to become hot. As fluid passes over the device it cools the wire and removes some of its heat energy, see Fig. (8).

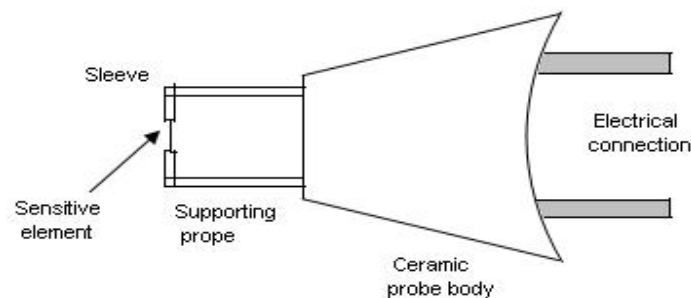


Figure 8: Thermo-anemometry probe

<http://www.tutorhelpdesk.com/homeworkhelp/Fluid-Mechanics-/Hot-Wire-Anemometer-Assignment-Help.html>

Thermo-anemometers can be operated in either constant current or constant temperature configurations. In the constant current mode there is a danger of burning the wire if the fluid flow rate is very low. Also if the fluid flow rate is very high the data acquired will not be accurate enough because the wire will not be heated enough to give a data describes the flow conditions. For these reasons and more most of hot-wire anemometers are used in a constant temperature configuration. The main configuration of the hot wire anemometry device is mainly depends on transduce elements which is can be done by the probe and wire then the signal processing and later the data analysis, see fig. (9).

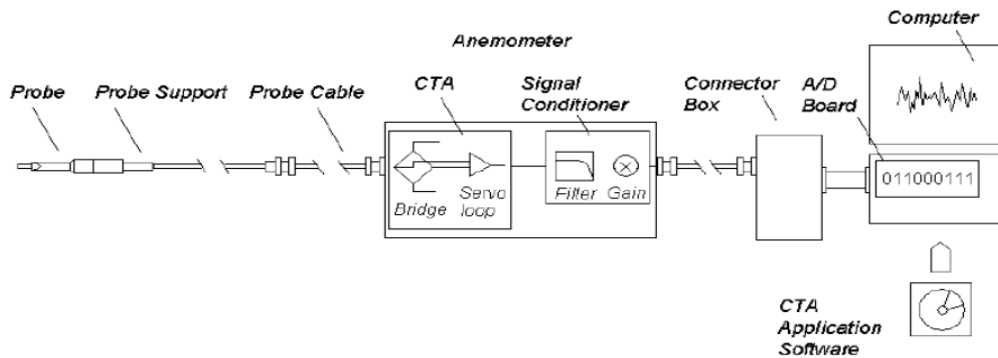


Figure 9: Signal processing in thermo-anemometry by Csaba Horváth hot wire anemometry lecture

To obtain the most accurate data possible hot-wire anemometers are typically used as part of a Wheatstone bridge configuration. An example of a constant temperature Wheatstone bridge circuit is shown in fig. (10).

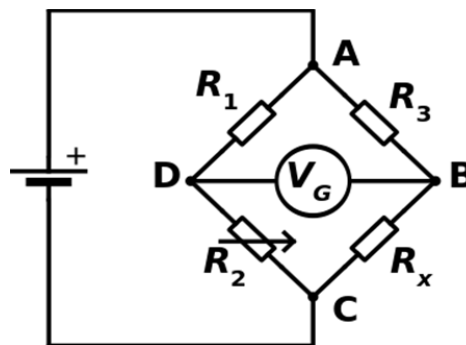


Figure 10: Wheatstone bridge circuit [https://en.wikipedia.org/wiki/Wheatstone\\_bridge](https://en.wikipedia.org/wiki/Wheatstone_bridge)

The circuit is composed of two known constant resistors and  $R_1$  and  $R_2$ . The third resistor is variable resistor  $R_3$  and the fourth resistor which completes the bridge is  $R_4$ . The bridge should be balanced to avoid any voltage error which may affect the real readings of the Wheatstone bridge [31]:

$$\frac{R_2}{R_1} = \frac{R_x}{R_3} \quad (8.4)$$

To understand the relationship between the current and the flow velocity it is necessary to solve the heat balance equation for the wire

$$H_g = H_R + H_A + H_c + H_{conv} \quad (9.4)$$

where,  $H_R$  is heat from radiation,  $H_c$  is heat by conduction and  $H_{conv}$  is heat by convection which is most important. For steady state conditions there is no heat accumulation  $H_A$  in the wire so this term goes to zero. The heat generation,  $H_g$  by joule heating is a function of the electrical current.

$$H_g = I^2 R_w \quad (10.4)$$

Where,  $I(A)$  is the current through the circuit and  $R_w(\Omega)$  is wire resistance at temperature  $T_w$

So we can state that 
$$I^2 R_w = h A (T_w - T_a) \quad (11.4)$$

Since 
$$Nu = \frac{h d}{k} \quad (12.4)$$

So 
$$I^2 R_w = \frac{A}{d} Nu K (T_w - T_a) \quad (13.4)$$

where,  $Nu$  is Nusselt number,  $D$  is diameter of the wire,  $A$  is area of heat transfer,  $T_w$  is wire temperature in K and  $T_A$  is fluid temperature in K

$$Nu = 0.42 Pr^{0.2} + 0.57 Pr^{0.33} + Re^{0.5} \quad (14.4)$$

$$Pr = \frac{\mu c_p}{k} \quad (15.4)$$

$$Re = \frac{\rho U d}{\mu} \quad (16.4)$$

The wire resistance as a function of temperature can be described by the following series

$$R_w = R_0 [1 + C (Q_w - Q_0) + C_1 (Q_w - Q_0)^2 + \dots] \quad (17.4)$$

where,  $R_0$  is wire resistance in a reference temperature,  $T_0$  is initial wire reference temperature and  $C$  is temperature coefficient of resistivity

$$H_t = h A_s \Delta q \quad (18.4)$$

Thus substituting the value of Nusselt number and expressing temperature as a function of resistance and doing some algebraic manipulation we get

$$H_t = (R_w - R_g) (X + Y\sqrt{U}) \quad (19.4)$$

where

$$X = \frac{0.42 K A_s}{R_0 C_d} \left(\frac{\mu C_p}{K}\right)^{0.2} \quad (20.4)$$

$$Y = \frac{0.57 K A_s}{R_0 C_d} \left(\frac{\mu C_p}{K}\right)^{0.33} \left(\frac{R d}{\mu}\right)^{0.5} \quad (21.4)$$

By substituting in equation 13 we get the following expression

$$I^2 = \left(\frac{R-1}{R}\right) (X + Y\sqrt{U}) \quad (22.4)$$

or

$$I^2 = A + B\sqrt{U} \quad (23.4)$$

which is so called King's law for calibrating hot wire anemometer.

## 5 Chapter Five: Design and construction of the experiment

The experiment was focusing on studying the wake of the bluff body which was chosen to be circular cylinder. Also the study is aim to focus on the he wake in water as medium of the movement of the cylinder. In this section it will be discussed the experimental techniques and facilities used to get the results. The design was made according o some previous theoretical considerations used by previous publishers. I tried to choose the dimensions of the equipment as close as I can to the previous works by other publishers in order to get a good validation to them results.

### 5.1 Experimental apparatus and techniques

The experiments were held in the laboratories of the technical university of Liberec and materiel was brought by the machine and energetic equipment department. A towing tank was used to perform the experiment. The dimensions of the towing tank were length  $\times$  width  $\times$  height (500  $\times$  110  $\times$  110) cm, [26]. The test section consists of 15 mm thick glass windows held together by a steel frame so the towing tank is optically accessible from all directions. These plates are constructed such that during their translation a minimum of disturbances is created. Salted water was used to increase the electrolysis process in the water tank. The tank was prepared with draining tab and filter to avoid any leakage of the toxic material to the plumb water, see fig. (11).

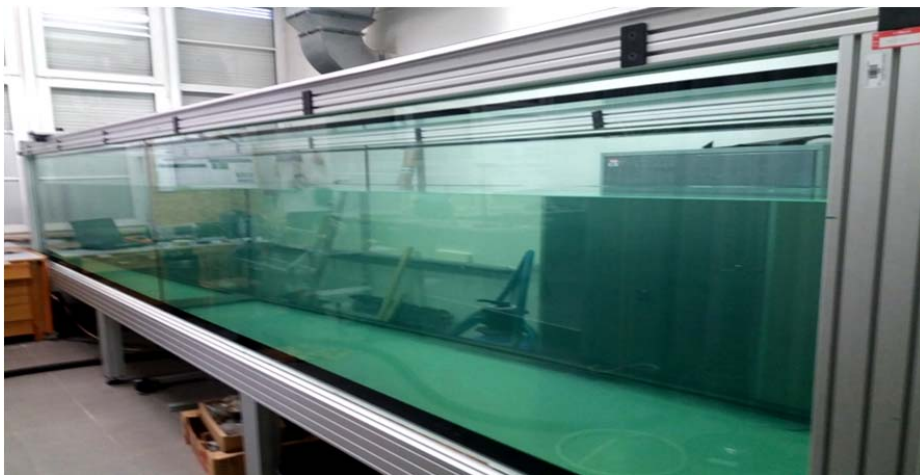


Figure 11: Towing tank

The cylinder was designed from an aluminum tube with external diameter  $d = 10$  mm. Cylinder was positioned between two Plexiglas plates which are connected to a stiff construction

on which different kinds of measuring equipment like cameras and light sources can be placed. The cylinder was equipped with end cylinders made of stainless steel with a diameter of 10 mm on both ends. The presence of end cylinders and end plates should ensure parallel vortex shedding during the experiment. Also minimum disturbances are created and oblique vortex shedding is suppressed. The diameter of the end cylinders is recommended in the range of  $D = 1.8d: 2.2d$  and the length of the end cylinders should be at least  $L = 5d$ . The free length of the cylinder between these two end cylinders was  $L = 400$  mm which corresponds to the aspect ratio  $\lambda = L/d = 45.3$ . The cylinder together with the end cylinders were attached between end plates. The stiff construction can be translated along two rails that are mounted on top of the water tank, See fig. (12).

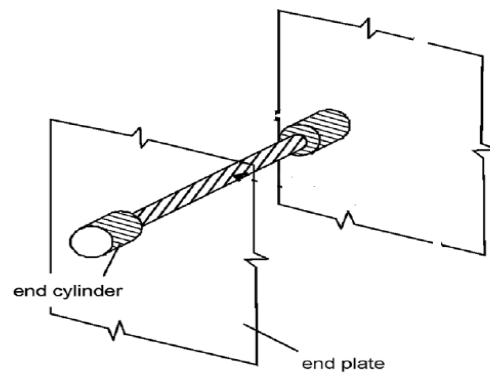


Figure 12: Construction of the end cylinders and the end plates

The distance between the cylinder and the bottom of the water tank and the free surface is, respectively,  $25D$  and  $50D$  blockage effects become negligible for distances larger than  $20D$ . It is assumed that a distance of  $50D$  is enough to rule out any influence on the buoyancy induced transition processes as investigated in the present study. The main source of error in the free-stream velocity is a result of the background velocity in the water tank which is caused by temperature differences in the water due to any external source like the laboratory room temperature. By conditioning this room and by thermally insulating the tank from the room, the background velocity could be minimized to 0.2 mm/s. Together with the other error sources this means an error in the measured velocity (at  $Re_D = 117$ ) of 2.0%. The wavelength of this background velocity was about the tank width = 50 cm. [33]

the design holders was selected to be M 10 screw rods to give stiffness for the assembly and also ability to change the positions of the clamps which was connected to the screw rod and from the other side lifting the end plates horizontally. The design was mounted on an aluminum profile which was situated horizontally over the Motor rails to transport the movement to the assembly. The assembly was made in the thermo-anemometry lab.

The Experiment was done in two positions in order to get to forms of vortex shedding in two different plans. The first was vertical cylinder moving through the test section. The second was to move the cylinder horizontally through the fluid. The same materials were used to perform the experiment in the two designs, See fig. (13) and, fig. (14).

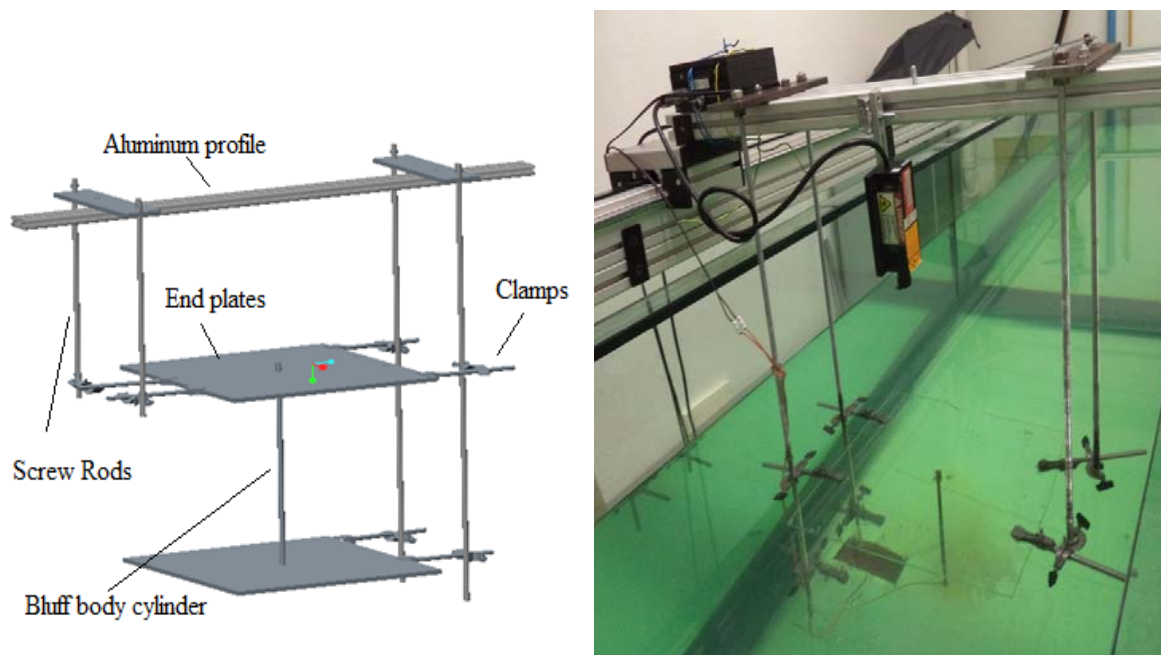


Figure 13: Experiment design in vertical cylinder mode





Figure14: Experiment in horizontal cylinder mode

## 5.2 DC Motor

The transition of the designed mechanism through the towing tank was performed by means of DC motor Maxon as an actuator. The Dc Motor transmitted the velocity to the mechanism by a pulley and belt which is connected between the two ends of the towing tank, Fig. (15). The motor was powered by AC/DC power supply up to 40 VDC. The voltage is connected to an encoder which controls the velocity needed in RPM. The encoder was connected to pc software EPOS Studio 1.20. The RPM velocity was converted to Reynolds number by the equation.

$$\text{RPM} = \frac{R_e \times \mu}{1.675 \times 10^{-4}} \times 4860$$

where,  $R_e$  is Reynolds number and  $\mu$  is kinetic viscosity at the laboratory temperature.

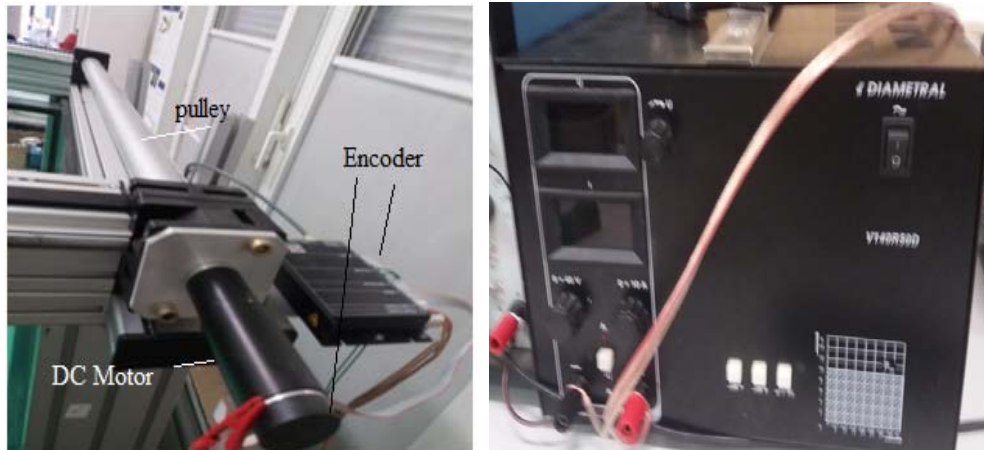


Figure 15: a) DC motor components, b) power supply

### 5.3 Laser Device

The method of illuminating the hydrogen bubbles generated by the tin ion electrolysis was to use a laser light sheet directed to the required plane which we want to visualize. The laser sheet thickness was typically 1 mm, [16]. It was obtained by covering the laser beam with aluminum adhesive tab with only hollow strip with required thickness. In this way also quantitative information could be obtained from the visualization results. The laser device was attached to the aluminum from with possibility to move it span wise to get gain different information from any plan intended of the measuring process. The frequency of the laser beam was selected to be 200 Hz and the onset to 501 mV, see fig. (16).

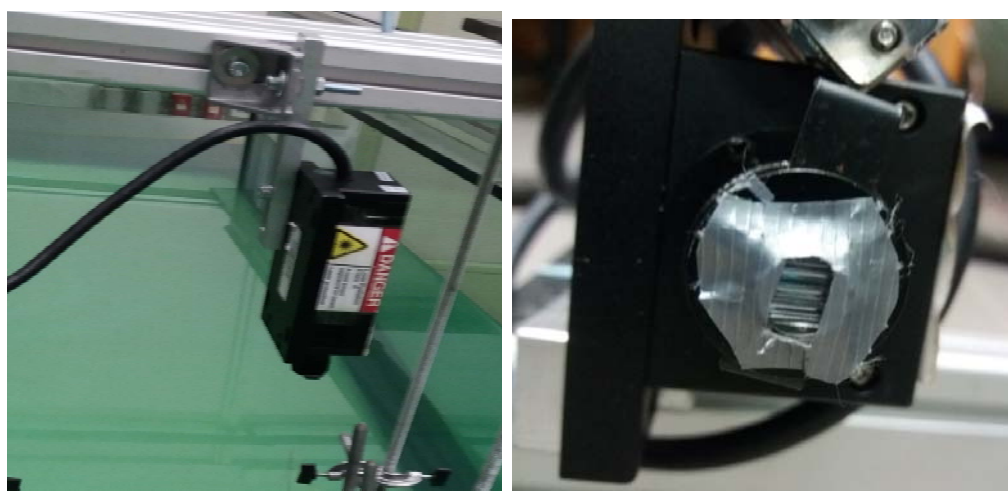


Figure 16: a) mounted laser device, b) slotted adhesive aluminum tab on the laser lamp

## 6 Chapter Six: Results and Discussion

A result was taken from the experiment in two different orientations and in four different velocities 30, 50, 90 and 120 Reynolds number. The main target is to study the vortex shed after the cylinder in two planes. The first plan is visualized by setting the vertically and mounting the laser beam in the top of the towing tang in a direction horizontal to the direction of the cylinder movement direction. The second was performed by mounting the laser beam in a direction vertical to the cylinder movement axes.

### 6.1 Experiment at $Re = 30$

Here the flow is in the attached eddies regime. During the visualization of the flow in  $Re = 30$  it was observed that the flow was Laminar flow, see fig. (17). The flow along the span wise of the cylinder was parallel. The separation point of the flow happened at the downstream side with an angle approximately  $135^\circ$  from the front stagnation point. There are two attached vortices past the cylinder surface. There was not von Kármán vortex formed as expected since the von Kármán vortex shedding is usually starting after  $Re = 47$ , [34].

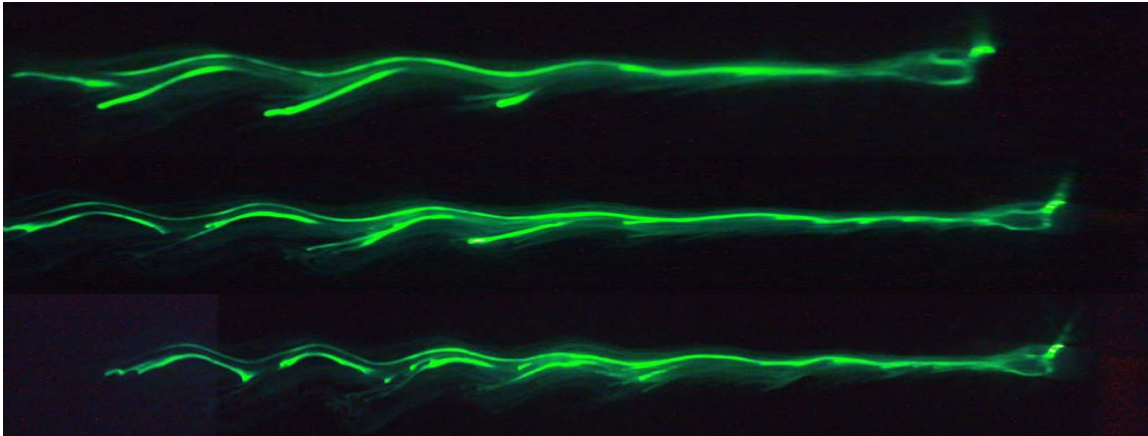


Figure 17: Side view of the vortex shedding from the cylinder movement at  $Re=30$

For the span wise view of the cylinder, it was observed that the fluid stream flows over the cylinder and gather after the cylinder again to flow horizontally in the plane of the flow stream. There is separation between the cylinder body and the point of fluid reattachment due to the von Kármán small vortices which is attached to the cylinder. Circular vortices are appearing past the cylinder and disappearing in the rear of the flow, See fig. (18).

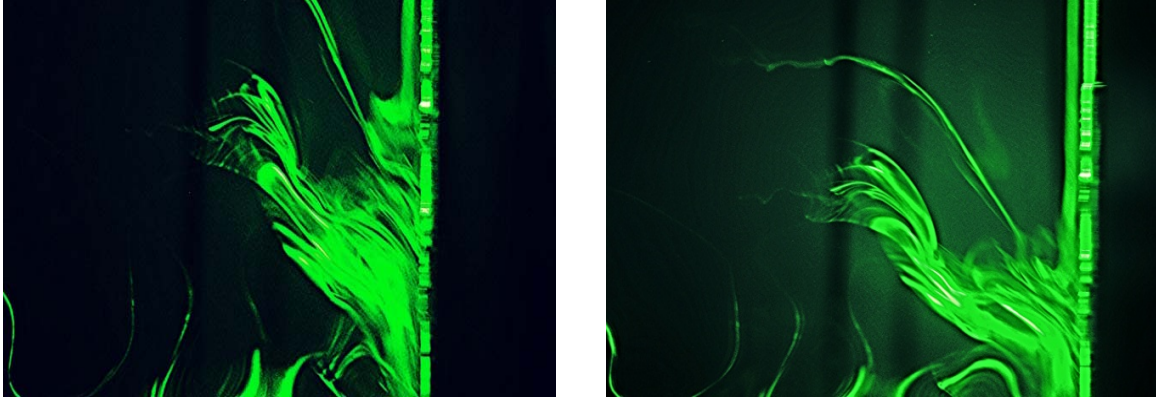


Figure 18:  $Re=30$  top view of the vertical cylinder span wise vortex shedding

## 6.2 Experiments at $Re = 50$

Using Reynolds number  $Re=50$ , von Kármán vortex started to present in the flow past the cylinder. This Reynolds number is in the onset of von Kármán regime at the low  $Re$  range which is so called the wake instability regime. From the side view we can visualize clearly the von Kármán vortex in a low frequency due to the relatively low velocity which satisfies the Strouhal number direct relation with Reynolds number value. Moreover, the stagnation point of the flow separation was observed to be at  $0$  degree with the flow stream axes. The separation point is in the downstream side with angle approximately  $125^\circ$  from the front stagnation point counter clock wise. The separation angle was observed to have fluctuation of about  $1^\circ$  to  $2^\circ$  with time. The von Kármán vortices were shedding alternatively between the two sides of the flow stream in a constant frequency along the cyclic length. The size of the von Kármán vortices was relatively small in both sides. The distance also between the vortices in the vortex shedding train was relatively long and the linear axis of motion of the vortices was parallel to the flow stream, see fig. (19).



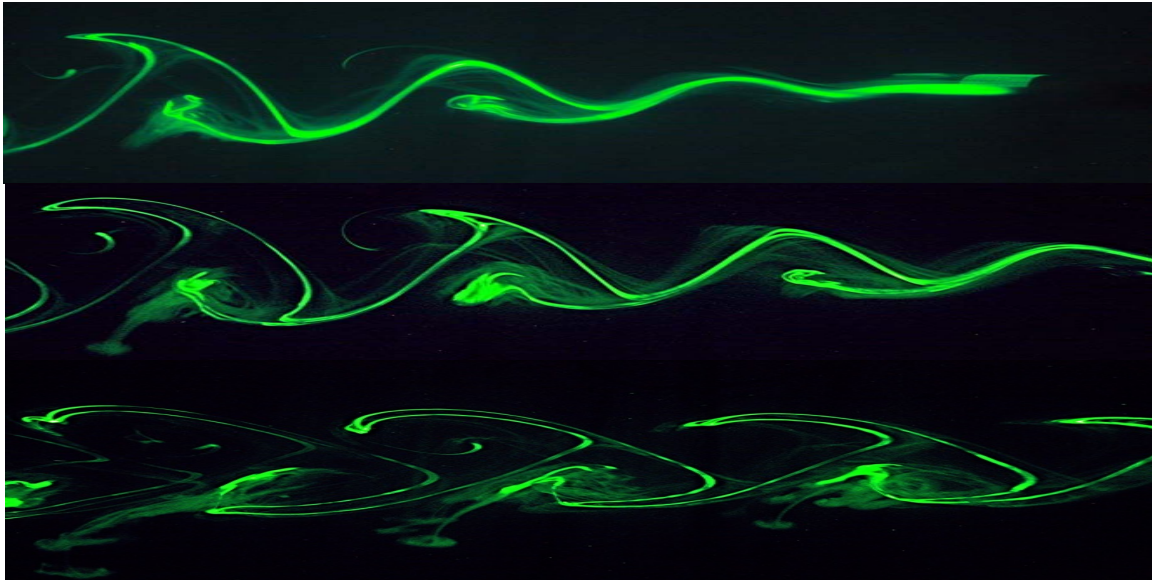


Figure 19: Stream wise view of the vortex shedding street from the cylinder linear motion at  $Re=50$

From the span wise view we can see that the flow past the cylinder is parallel with some oblique waves in the two ends which is so called quasi periodic oblique mode. The frequency in the middle cell of the flow has higher frequency than the frequency of the end cell. In the bottom we can see that the waves are almost not identified due to the low frequency of the cell in addition to the end effects. The wave length is a little bit long in comparison to higher velocities which explain the big size of von Kármán vortices in the side view, see fig. (20).

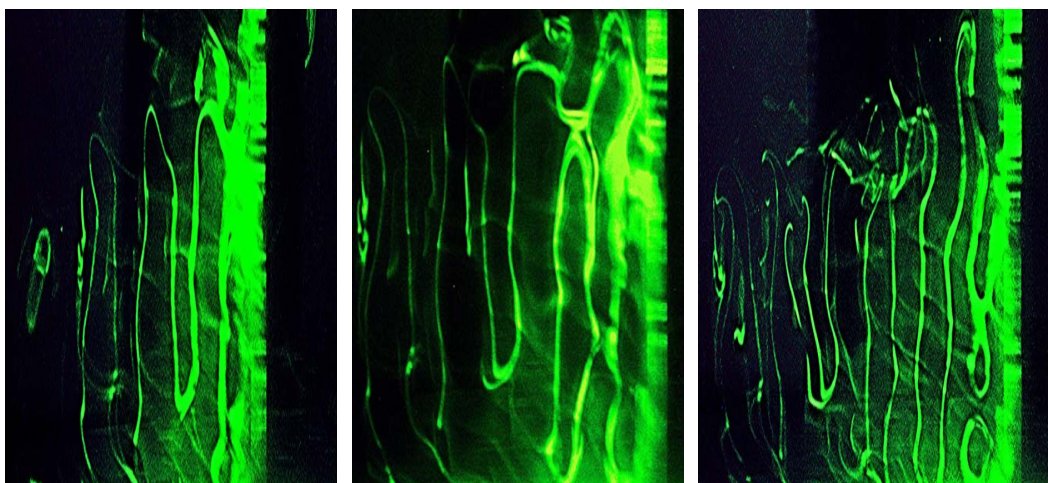


Figure 20: Span wise view for the wake of the cylinder at  $Re =50$  flow from right to left

### 6.3 Experiments at $Re = 90$

The flow in this Reynolds number is present in the transition between the onset of von Karman flow regime and the pure von Karman vortex shedding regime. From the stream wise view we can see that it satisfies the vortex shedding mode. We can see regular vortex street in regular frequency between the top and lower vortex street. It is observed that the separation angle is smaller than the corresponding angles in previous velocities. We can estimate it approximately in the range of  $110^\circ$ . We can observe the stagnation angle of the flow around the cylinder at  $0^\circ$  from the stream wise axes. The strength of the vortices in the upper and lower street is almost the same with smaller size than the previous velocities. The relative motion between the each vortex and the following one is almost the same along the cycle length, see fig. (21)

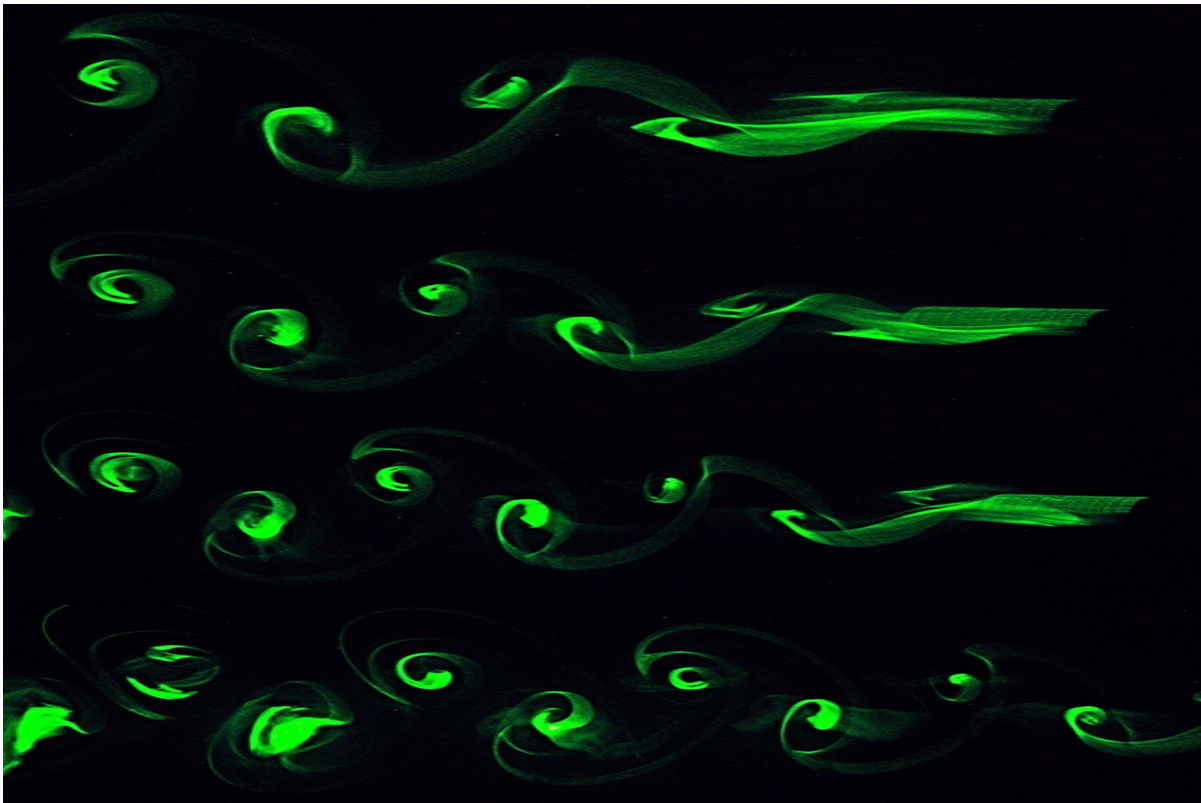


Figure 21: Stream wise view of the vortex shedding street from the cylinder linear motion at  $Re=90$

If we have a look on the cylinder span wise view we can see the periodic oblique shedding mode. There are two frequencies existing in the flow the first one is the frequency of the middle

cell which is higher than the frequency at the end cells at the two sides of the flow. The oblique front line is the imaginary line connecting the oblique shedding with the parallel shedding. It can be observed that the connection between the oblique wave and the parallel wave is curvature not a sharp connection. The possible reason the oblique shedding exists in one end and disappearing in the other end is possibility of the not perfectly horizontal one end plate orientation during the installation. We can see also that the wavelength of the vortex shedding is smaller than the lower Reynolds number and higher frequency in the same cyclic length. The flow direction is from right to left and distance traveled by the cylinder is  $50D$ , see fig. (22)

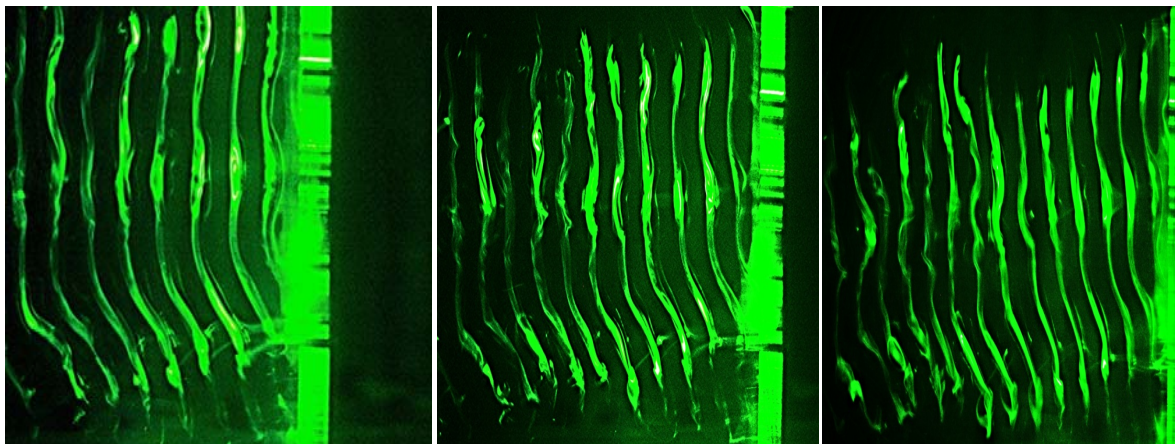


Figure 22: Span wise view for the wake of the cylinder at  $Re = 90$  flow from right to left

#### 6.4 Experiments at $Re = 130$

The flow velocity of  $Re = 130$  is pure von Kármán vortex regime. We can observe clearly that the frequency of the vortex shedding past the cylinder is higher due to the higher Reynolds number. The separation angle is almost  $100^\circ$ . The frequency past the cylinder is higher than in the rear of the flow and the possible reason for that is high friction drag which consume the flow energy. The relative motion between the cascading vortices is not constant and the vortices started to move in two dimensional vector velocities in both the span wise direction and the stream wise direction. According to Roshko [35] the wake width past the cylinder is a function of the Reynolds number. The increase in Reynolds number consequently decreases the wake width and induces the free vortex layer to converge to the inward direction unlike the ideal state of the flow. Roshko analyses also stated that drag forces is related to the low pressure region



in the wake. The after pressure also is one reason because the negative pressure past the cylinder is increasing which induces the flow naturally to move to the lower pressure area which is causing the free vortex layers convergence. The size of the vortices also is getting smaller with higher centrifugal velocity, see fig. (23)

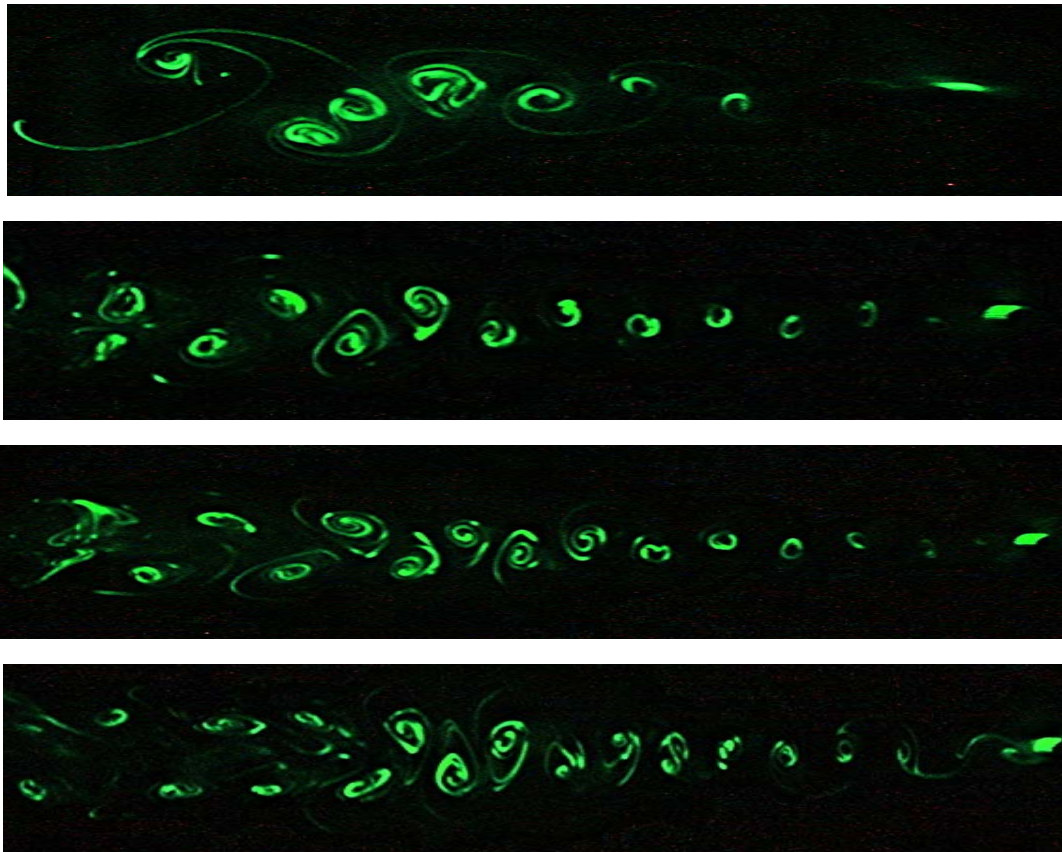


Figure 23: Stream wise view of the vortex shedding street from the cylinder linear motion at  $Re=130$

Regarding the span wise view of the cylinder it was observed that the shedding includes two different shedding frequencies. Consequently the shedding past the cylinder was divided in to two modes (oblique, parallel) shedding. In the second photo we can observe vortex dislocation exists in the bottom of the wake near the cylinder body. This dislocated vortex will connect with two another vortices which have the same sign in order to form parallel shedding mode in the fourth photo. This dislocation phenomenon agrees with the observations of Browand and Prost-Domasky [36], see fig. (24).



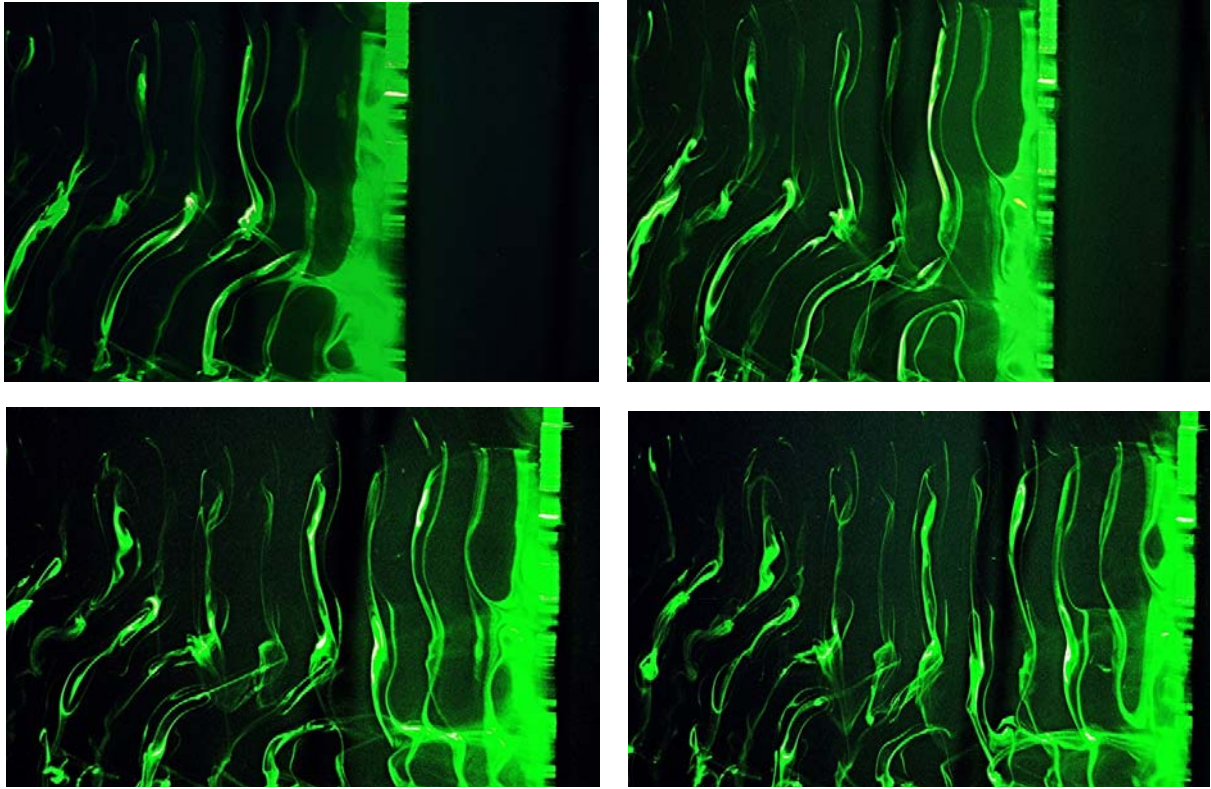


Figure 24: Span wise view for the wake of the cylinder at  $Re = 130$  flow from right to left

## 7 Chapter Seven: Comparison of current results with previous authors results

Getting acceptable results through the experimental work will not be sufficient without comparing and finding the discrepancies with previous author's results and hypotheses about similar situation like the current research work. The studies of fluid past flows past circular cylinders have been evolved so much in the recent thirty years due to the extensive researches done on such flows like this which in turn resulted in so big advancement of the quality and areas of the topic studied.

The results got by the experiment agrees with the claim of (Park et al., 1998; Fey et al., 1998; Norberg, 2001) that what is so-called the von Kármán vortex shedding start to appear after  $Re > 47$  and less than this value the flow tends to attach again in the streamline direction. The experiments at  $Re=30$  shows the presence of two attached eddies to the cylinder which confirms the numerical investigations done by (Masami Sato, 2012) which states that the two similar vortex past the cylinder start to appear at  $Re = 20$ . The discrepancy was the size of the two eddies attached to the Reynolds number which was in my case not similar in the size due to the inequality of the strength of the two eddies, see fig. (25)

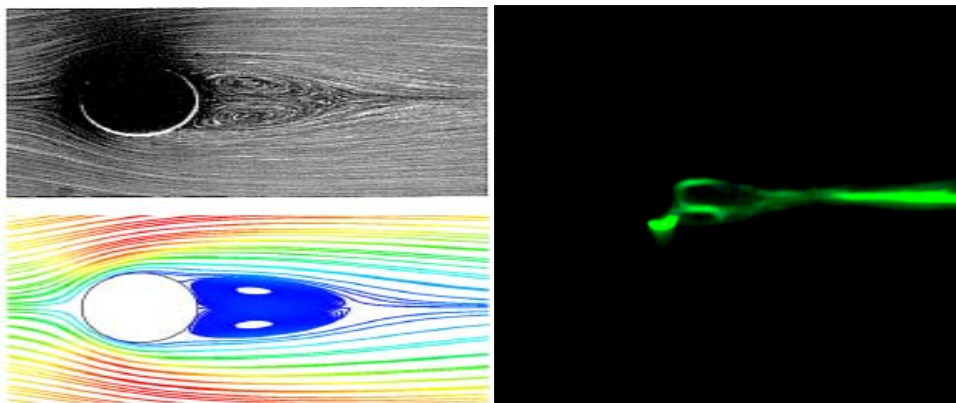


Figure25:  $Re=30$  Comparison of a) numerical and experimental investigations by Masami Sato, b) current experimental results carried out for this thesis

The detection of the stagnation, separation and reattachment points was observed by (Rajani B. N., 2005) numerical work. He observed that the stagnation points tends to be 0 for the range of Reynolds numbers  $0 < Re < 50$  and that it will oscillate periodically around 0 with the value of

$\pm 0.67$  to  $\pm 2.166$  for the range of Reynolds numbers  $50 > Re > 200$ . These results agree to the detections gained by the current experimental work. He also observed the separation points angle in the range of Reynolds numbers  $50 > Re > 5000$ . He proposed that the velocities up to  $Re = 50$  tends to result separation angle of  $123.6$  while in the current experimental work it was observed the stagnation angle in the range of  $\theta_s = 135$  for  $Re = 30$  and  $\theta_s = 120$  for the  $Re = 50$ . For higher Reynolds number it was found numerically that for  $Re = 80$   $\theta_s = 119$  and for  $Re = 100$  it was found that  $\theta_s = 116$  which is showing discrepancy for the observed results by the current experimental work. The following diagram shows the relation between Reynolds number and separation angle stated by some other authors, see fig. (26).

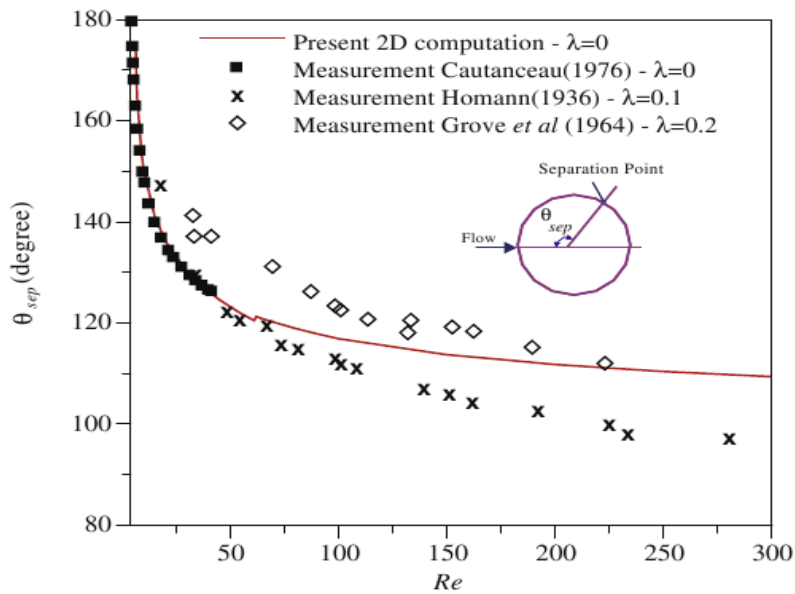


Figure 26: Relation between Separation angle and Reynolds number by several authors (B.N. Rajani, 2009)

The frequency of the von Kármán vortex shedding which is represented in the form of Strouhal number was investigated by several authors starting from (Zdravkovich -1997) and the proposed calculations which was performed by Rayleigh and Roshko vs. the Reynolds number in addition to the numerical simulation by Masami Sato all agree that direct relation between Strouhal number and Reynolds number which can be observed clearly by the current experimental results, see fig. (27).

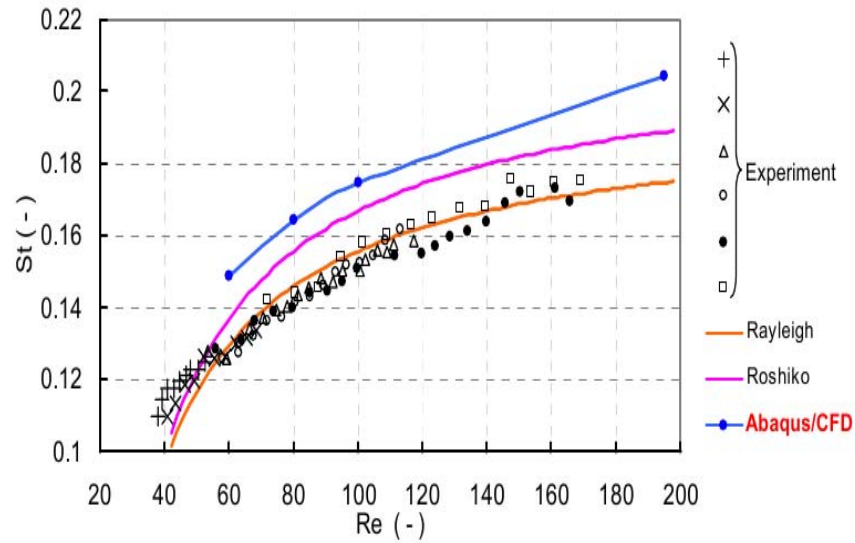


Figure 27: Variations of Strouhal number vs. Reynolds number by Masami Sato 2012

For Reynolds number less than 40 the flow over the circular cylinder reaches the steady state within 15 second and two symmetric vortices are formed behind the cylinder (Braza et al, 1986) which is visible at  $Re=30$  that there is still some disturbance in the flow stream even after the passing of the cylinder. The von Kármán vortex shedding was obvious at  $Re=50$  in which agrees with (Nishioka sato, 1974) and (Provansal and Boyer, 1984).

The relation between vortex size, circulation length and Reynolds number was investigated numerically by (B.N. Rajani, 2009) and experimentally by (Coutanceau and Bouard) and it was discovered the direct relation between the circulation length and Reynolds number and the inverse relation between the size of the vortex and Reynolds number. The experiments were done on low Reynolds numbers these results considerably agrees with the current experimental work.

The span wise flow investigations done by (Williamson, 1989) was mainly to study the oblique vortex shedding modes and the phenomenon accompanying it. In the lower oblique vortex shedding mode Reynolds number range (quasi periodic mode),  $Re=50$  was performed in the current experimental work. In comparison to Williamson's experimental investigation in the same regime we can see some discrepancies between the two results. The main difference is the

two vortices shedding frequencies in the two sides of the span. The reason for this difference may be arise due to the end effects in Williamson model which affected the results. One other possible reason for the difference in the recorded results is the different orientation of the cylinder in the flow. In the current research the cylinder was mounted vertically in the flow while in Williamson model it was used in horizontal orientation in the flow. One more reason for the discrepancies which may affect the results is the aspect ratio difference between the two experiments models. Williamson used aspect ratio  $\lambda = 70$  while in the current work  $\lambda = 45.3$ , see fig. (28).

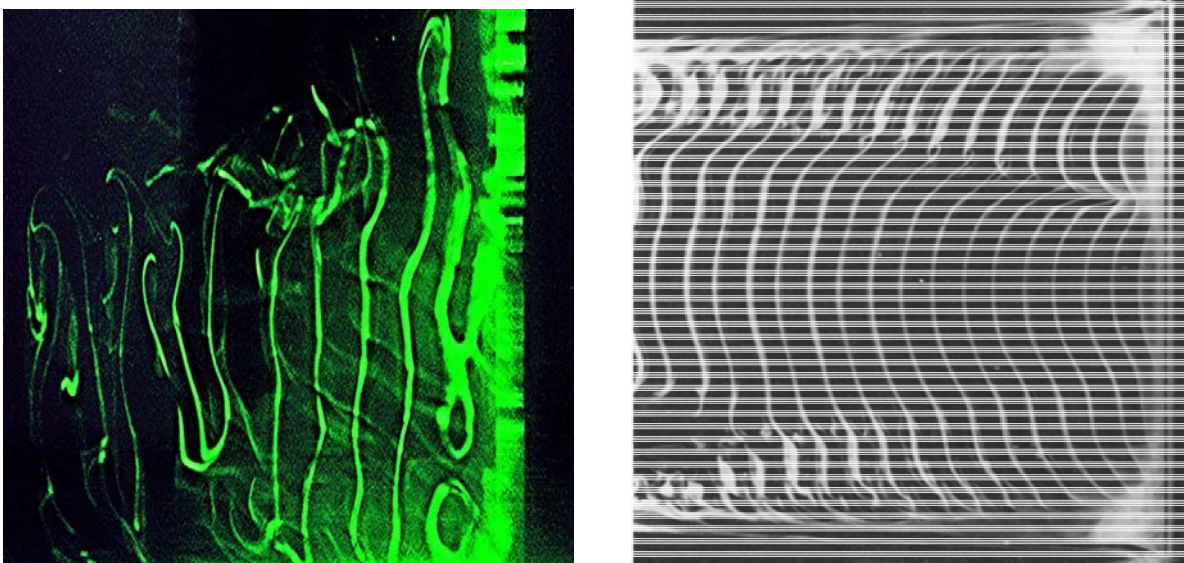


Figure 28: Quasi periodic oblique shedding regime a) present work  $Re=50$ , b) Williamson, 1986  $Re=64$

For the higher oblique shedding mode it was observed considerably large agreement between the two results between the current work and the work done by Williamson. We can see the presence of the parallel vortex shedding in the two cases. In the current work the chevron shape can be seen clearly in on side and with lower grade in the other side while in Williamson's work it is very obvious the chevron shape. The reason for this small difference as mentioned in the previous chapter is the positioning of the end plate which probably affected the angle of the chevron shape, see fig. (29).



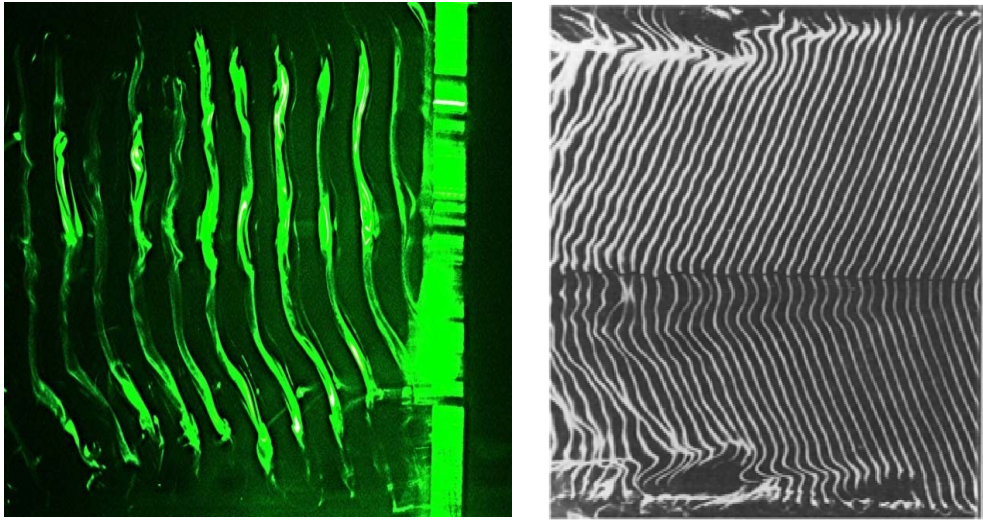


Figure 29: Periodic oblique shedding mode a) present work  $Re=90$ , b) Williamson's work 1986  $Re=85$

Williamson did his experiment to prove the effect of the end plates on the angle of the oblique wave. His results approve that that with a little change in the angle of the end plate angle we can get significant resultant oblique angle in the vortex shedding. The application of this kind of tilting from one side affects the other side of the change only without any effect on the side of span next to the tilting action, see fig .(30).

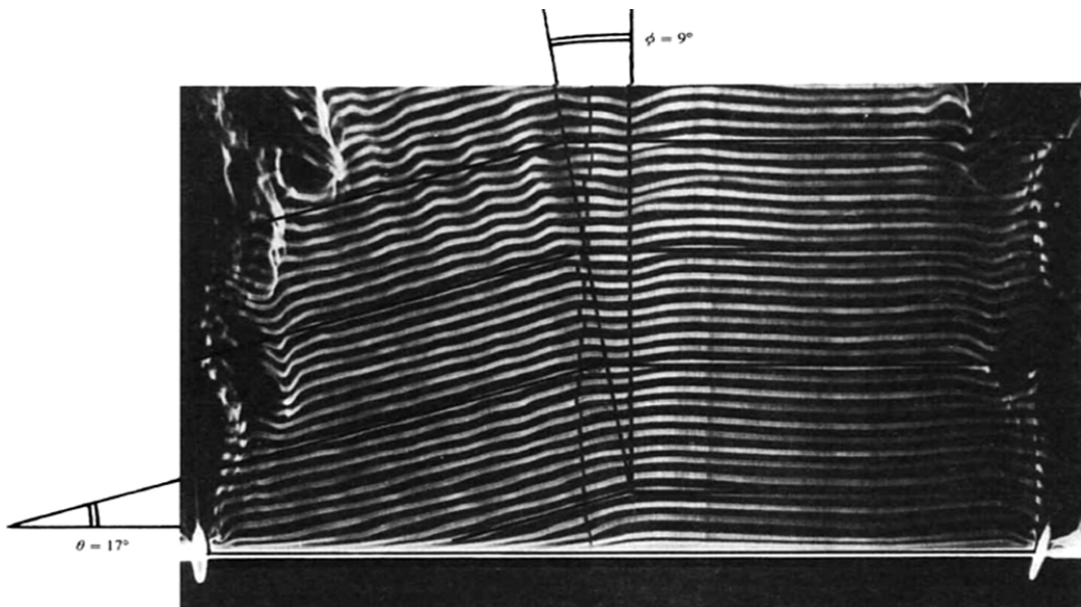


Figure 30: Effect of tilting the end plate on the oblique angle  $Re=90$ , Williamson 1986

For higher velocities in the oblique shedding mode it was observed some dislocation present in the vortices shedding waves. We can see as mentioned before the dislocation took effect in the bottom of the photo in one wave and the dislocated branch of the wave started to attach to the following wave. The same happened with Williamson's model we can see some dislocations in the bottom of the move and the dislocated branches started to connect with following branches, see fig. (31).

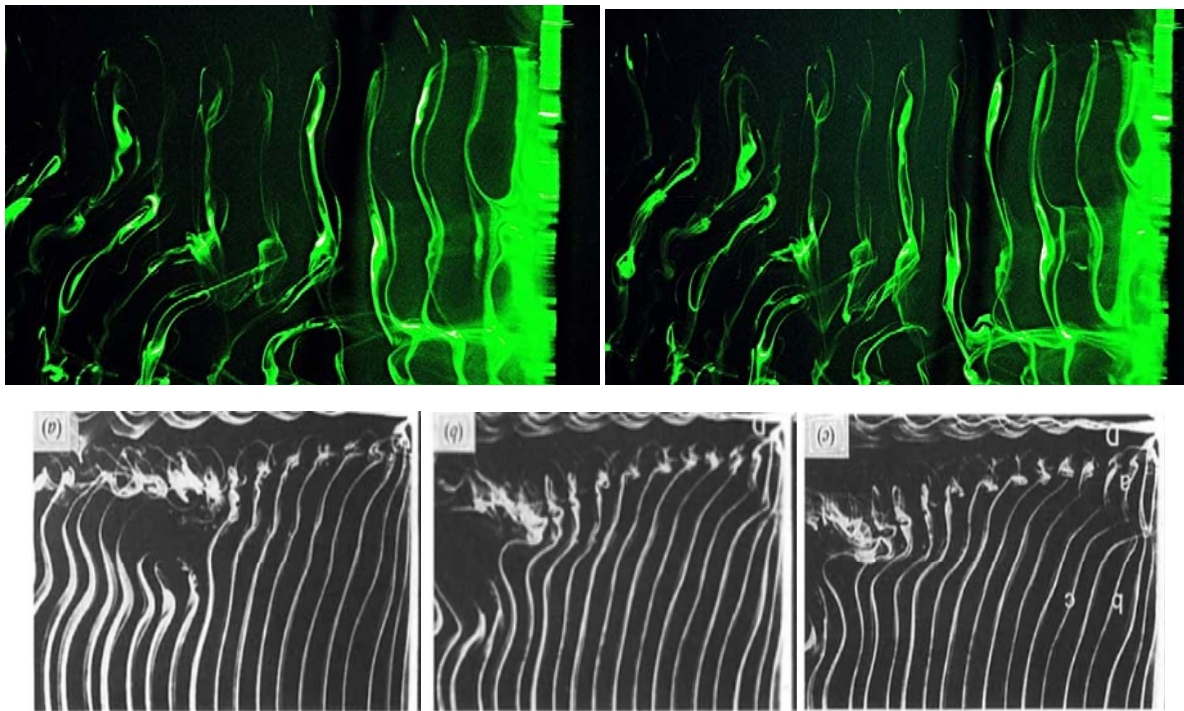


Figure 31: Development over one beating cycle of a vortex dislocation near the bottom end of the cylinder span a) present work  $Re=130$ , b) Williamson's experiment  $Re=100$

## 7.1 Future work

The current thesis work is starting point for a future advanced work in the field of von Kármán vortices and its applications. For the coming future work either in my Ph.D. studies or researches, advanced investigations could be done on von Kármán vortex shedding and the phenomenon accompanying it. The investigations could be about studying the behavior of the flow experimentally and numerically regarding the velocity, pressure and drag forces distribution and the effect of the body shape and velocity on these variables. Some practical applications of the von Kármán vortices can be investigated and applied in the laboratory in addition to studying

the methods of advancing the applications designs. Further experimental methods can be used to advance the ability to investigate the flow in more accurate way and getting more realistic results in order to validate the results gained experimentally and numerically.



## 8 References

- [1] A. Sohankar. 2007, *Hopf bifurcation, vortex shedding and near wake study of a heated cylinder in gross flow*. Iranian Journal of Science and Technology, Transaction B, Engineering, Vol. 31, No. B1, pp 31-47
- [2] V. Kármán, 1911. *Über den Mechanismus des Widerstands, den ein bewegter Körper in einer Flüssigkeit erfährt*. Ciittinger Nachrichten, Mat. Phys. Kl. pp. 509-517.
- [3] P.G. Saffman, J.C. Schatzman. 1981. *Properties of a vortex street of finite vortices*. SI AM J. Sci. Stat. Comp., 2:285-295.
- [4] S.R. Ahmed, G. Ramm, G. Falin. 1984. *Some salient features of the time-averaged ground vehicle wake*. SAE Technical Paper. 840300.
- [5] M. Provansal, C. Mathis, L. Boyer. 1987. *Benard-von Kármán instability: transient and forced regimes*. J. Fluid Mech., 182, 1-22.
- [6] P. W. Bearman, D. M. Trueman. 1972. *An investigation of the flow around rectangular cylinders*. Te Aeronautical Quarterly 23, 229 - 237
- [7] T. Mizota, A. Okajima, 1981. *Experimental studies of time mean flows around rectangular prisms*. Journal of the Japan Society of Civil Engineering, 39- 47 (in Japanese).
- [8] C. H. K. Williamson, 1986. *Oblique and parallel models of vortex-shedding in the wake of a circular cylinder at low Reynolds number*. Journal of Fluid and Mechanics 206, 579 - 627.
- [9] L. Schibuola. 1999. *Experimental analysis of a condenser heat recovery in an air conditioning plant*. Energy 24, 273-283.
- [10] K. Shimada, Y. Meng. 1998. *Numerical analysis for the aerodynamic statistics of rectangular cylinders and aeroelastic vibration of  $B/D^2$  rectangular cylinder by k e model*. Proceedings of the 15th National Symposium on wind Engineering, pp. 161- 166 (in Japanese).
- [11] P. J. Strykowski, K. R. Sreenivasan. 1990. *On the formation and suppression of vortex shedding at low Reynolds numbers*. J. Fluid Mech. 218, 71–107.

- [12] H. Choi, W. Jeon, K. Jinsung. 2008. *Control of Flow over a Bluff Body*. Annual Review of Fluid Mechanics. 113-130. 4
- [13] H. Park, D. Lee, W. Jeon, S. Hahn, and J. Kim. 2006. *Reduction in flow over a twodimensional bluff body with a blunt trailing edge using a new passive device*. The Journal of Fluid Mechanics, 389-414.
- [14] M. Paley. 2000. *Stable periodic vortex shedding studied using computational fluid dynamics, laser sheet flow visualization, and MR imaging*. Magnetic Resonance Imaging 18, 473– 478
- [15] W.J.P.M. Maas, C.C.M. Rindt, A.A. van Steenhoven. 2003. *The influence of heat on the 3D-transition of the von Kármán vortex street*. Int. J. Heat Mass Transfer 46, (16) 3069–3081.
- [16] T. Vit. 2007. *The influence of temperature gradient on the Strouhal–Reynolds Number relationship for water and air* Experimental Thermal and Fluid Science. Vol. 31, No. 7, p.751
- [17] B.N. Rajani, H.G. Lanka, S. Majumdar. 2005. *Laminar flow past a circular cylinder at Reynolds number varying from 50 to 5000*. NAL PD CF 0501.
- [18] A. Venugopal, 2011. *Influence of blockage and shape of a bluff body on the performance of vortex flowmeter with wall pressure measurement*. Journal of the International Measurement Confederation
- [19] M. Sato, T. Kobayashi. 2012. *A Fundamental study of the flow past a circular cylinder using Abaqus/CFD*. SIMULIA Community Conference.
- [20] Zaaraoui. 2013. *A High Accuracy Volume Flow Rate Measurement Using Vortex Counting”* Flow Measurement and Instrumentation. Volume 33, Pages 138–144
- [21] L. Cheng, K. M. Lam. 2012. *Unsteady features of bluff body wake with application to building wake length*. The Seventh International Colloquium on Bluff Body Aerodynamics and Applications (BBAA7) Shanghai, China; 2-6.
- [22] H. Liang, 2015. *Span wise characteristics of flow crossing a yawed circular cylinder of finite length*. Procedia Engineering volume 126 pages 83 – 87

- [23] B. Siddhartha. 2013. *Experimental observation of boundary layer of the turbulent flow over a bluff body inside rectangular diffuser*. 5th BSME International Conference on Thermal Engineering, Procedia Engineering 56 275 – 280
- [24] N.R. Caetano. 2013. *Turbulent Flowfield Analysis in a Bluff-Body Burner Using PIV*. World Journal of Mechanics, 3, 215-223.
- [25] G. Buresti. 2000. *Bluff body Aerodynamics*. Proc. International Advanced School on wind excited and aero elastic vibrations of structure, University of Pisa, Italy
- [26] R.N. Kieft. 2000 *Mixed convection behind a heated cylinder*. Ph.D. Thesis, Eindhoven University of Technology.
- [27] J. H. Lienhard. 1966. *Synopsis of Lift, Drag, and Vortex Frequency Data for Rigid Circular Cylinders*. Technical Extension Service, Washington State University research division, bulletin 300
- [28] S , Taneda, H .Honji, and M .Tatsuno. 1977. *The Electrolytic Precipitation Method of Flow Visualization*. In, Proc. of the Intern. Symp. On Flow Visualization, ed. T. Asanuma, 133-138, Tokyo, Japan.
- [29] C. Brossrad, J.C. MONNIER, P. BARRICAU. 2009. *Principles and Applications of Particle Image Velocimetry*. Aerospace Lab n°1.
- [30] R. J. Adrian. 1991. *Particle-imaging techniques for experimental fluid mechanics*. Ann. Rev. Fluid Mech. 23 261–304.
- [31] Virginia Tech Department of Aerospace and Ocean Engineering. 2012. *Aerospace Engineering Lab Notes: Hot Wire and Hot Film Anemometry*. accessible from  
<<http://www.aoe.vt.edu/simpson/aoe4154/hotwirelab.pdf>>
- [32] A. Perry. 1982. *Hot Wire Anemometry*. Oxford: Clarendon Press, 1983. ISBN. 9780198563273
- [33] W.J.P.M. Maas, C.C.M. Rindt, A.A. van Steenhoven. 2003. *The influence of heat on the 3D-transition of the von Kármán Vortex Street*. Int. J. Heat Mass Transfer 46 (16) 3069–3081.

[34] H. Eisenlohr, H. Eckelmann. 1989. *Vortex splitting and its consequences in the vortex street wake of cylinders at low Reynolds number*. Phys. Fluids A 1 (2) 189–192.

[35] A. Roshko. 1954. *On the Development of Turbulent Wakes from Vortex Streets*. National Advisory Committee for Aeronautics, Washington, D. C.

[36] F. K. Browand, S. A. Prost-domasky. 1989. *Experiment on pattern evolution in the 2-D mixing layer. To appear in New Trends in Nonlinear Dynamics and Pattern Forming Phenomena*” Ed. P. Huerre.